

Comparative study of robotic artificial actuators and biological muscle

Advances in Mechanical Engineering
2020, Vol. 12(6) 1–25
© The Author(s) 2020
DOI: 10.1177/1687814020933409
journals.sagepub.com/home/ade
 SAGE

Wei Liang¹ , Hao Liu¹ , Kunyang Wang¹, Zhihui Qian¹,
Luquan Ren¹ and Lei Ren^{1,2}

Abstract

Biological muscles exhibit a high level of integration, in which actuators, sensors and transmission elements can be included in one component. Artificial muscles or actuators refer to intelligent stimuli-responsive materials that could reversibly deform with the trigger of various external stimuli. These materials, which have attracted tremendous attention, produce natural muscle-like actuation performance and show promising applications in robotics. After an introduction of various actuator technologies that contribute to robotic applications, a comparative analysis of the main actuation parameter is provided. The comprehensive comparisons of each kind of artificial muscle are summarised, and the promising properties that are required in robotics are presented, which highlight the development of their actuation performances and the challenges that limit their further employments. Future developmental prospects and perspectives of artificial actuators are discussed.

Keywords

Robotics, artificial actuators, actuation parameters

Date received: 14 November 2019; accepted: 19 May 2020

Handling Editor: James Baldwin

Introduction

Actuators have an increasingly important role in robotics. Considerable development in industry and scientific research has occurred due to the remarkable progress and achievements in actuator technologies over the past decades. Actuators have been largely applied to robots such as walking machines, humanoid robots, manipulators and biomedical devices.¹

Traditional actuators, such as electric motors, are extensively applied for robotics that rely on propulsion, rotation, lifting and positioning and feature high specific power. The maximum power per unit mass of electric motors that use permanent magnets is 300 W/kg, which is twice higher when actively cooled.^{2,3} Hydraulic and pneumatic cylinder actuators, which enable inherent compliance, have also been proposed. These actuators exhibit simplicity, compactness and high compressibility.^{3–5} Regarding the power/weight

ratio, hydraulic actuators have maximum typical values of 1.6–2 kW/kg, which exceed those of electric motors, with a magnitude of 100 W/kg.⁶ These types of actuators enable robots to perform diversified and powerful tasks such as handling heavy weights, accurately positioning themselves, running, jumping and even performing backflips.^{2,7}

¹Key Laboratory of Bionic Engineering, Jilin University, Changchun, P.R. China

²Department of Mechanical, Aerospace and Civil Engineering, The University of Manchester, Manchester, UK

Corresponding authors:

Zhihui Qian, Key Laboratory of Bionic Engineering, Jilin University, Changchun 130022, P.R. China.

Email: zhqian@jlu.edu.cn

Lei Ren, Department of Mechanical, Aerospace and Civil Engineering, The University of Manchester, Manchester M60 1QD, UK.

Email: lei.ren@manchester.ac.uk



Creative Commons CC BY: This article is distributed under the terms of the Creative Commons Attribution 4.0 License (<https://creativecommons.org/licenses/by/4.0/>) which permits any use, reproduction and distribution of the work

without further permission provided the original work is attributed as specified on the SAGE and Open Access pages (<https://us.sagepub.com/en-us/nam/open-access-at-sage>).

Although great progress has been achieved, a large gap between conventional robots and natural organisms still remains.^{8,9} Many challenges, such as challenges pertaining to the materials, bio-inspired design and system integration, have appeared during the development of bio-inspired robots. One main problem is how the actuators and their topologies enable seamless interactions between human beings and robots and between robots and the physical world.¹⁰ To understand the versatile functionalities and compliant interactions of biological mechanisms, the differences between conventional actuators and biological muscle (actuators of animals) must be distinguished.

Conventional robots are based on rigid materials for actuation and load bearing, which means that human–robot and robot–environment interactions must be monitored and precisely controlled to avoid safety hazards to humans or the robot.^{11,12} In contrast to conventional actuators, biological muscles feature compliance, which enables the load distribution on the muscle to be spread over a larger area and increases the contact time and decreases the maximum impact stresses. The compliance originates from the viscoelastic material properties of biological muscles, including the ability to change their moduli, which enables energy dissipation and the maintenance of stability during dynamic loading. Furthermore, biological muscles can freely vary their stiffness, which enables them to effectively adjust their mechanical compliance to interact safely with humans and adaptively interact with varying physical environments.¹³

Typically, conventional robots consist of numerous rigid links, which are connected by separate hinge joints.¹⁴ Each joint is actuated and controlled independently by separate hardware, including motors, sensors and controllers. When a fixed trajectory is given to an end effector, the angle of each joint required to follow this path is computed by the inverse kinematic method. In addition to the contact force between the end effector and the human/environment, the output torque of each joint is calculated by the inverse dynamic method for different situations in real time.¹⁵ The strategy of biological muscles is different, in which actuation, transmission elements, proprioceptive sensing and control circuit and viscoelastic properties are integrated into one material architecture.¹⁶ Rather than controlling the holistic impedance through every joint output torque as controlled in conventional robots, animals utilise the morphology, material and constraints of the entire muscle structure to adapt the stiffness and damping to an unknown environment. This control concept is also known as morphological computation.¹⁷ Morphological computation integrates embodied intelligence into robots, which reduces the large amount of dynamic computation during real-time locomotion.

Therefore, differences in the actuation principle between conventional robot actuators and biological muscles still exist. To bridge the gap between conventional robots and biological systems (human and animals), the first and primary step is to select an appropriate actuation material that can achieve biological muscle performance. The ‘artificial actuators’ that are extensively employed in robotics have been developed to realise a light weight, miniaturisation, flexibility and can mimic biological muscles, which offers the opportunity to improve robots.²

This article identifies the artificial actuators that can perform as biological muscle. First, non-conventional artificial actuators that are extensively applied in robotics, including pneumatic artificial muscles (PAMs), shape memory alloys (SMAs), electroactive polymers (EAPs) and newly developed actuators. Conventional actuators, such as electromagnetic motors and hydraulic actuators, and infrequently employed artificial actuators, such as piezoelectric actuators, shape memory polymers and hydrogel actuators (HGA), have been reviewed or compared with muscles elsewhere.^{18–20} Then, the basic working principles, classifications and applications of the extensively applied artificial actuator technologies are introduced in section ‘Artificial actuator technologies’. In section ‘Results’, representative actuators of each technology are discussed and compared based on their actuation parameters. On one hand, the same parameters of these actuators are intercompared; on the other hand, the comprehensive actuation performances of these actuators are individually compared to that of biological muscle. The comparison results reveal the advantages and disadvantages of the introduced actuator technologies. Options for actuation are provided to satisfy different robotic application requirements, and suggestions for selecting suitable robotic actuators are offered. In section ‘Future directions’, the prospects of artificial muscles are proposed based on generally employed artificial actuators, which provide insights into future biomimetic design.

Artificial actuator technologies

In this part, four main artificial actuator technologies – PAMs, SMAs and EAPs – and newly developed actuators will be introduced. This study mainly discusses actuators that can be employed as actuators in robots, while other actuators fall into the categories of PAMs, SMAs and EAPs or newly developed actuators are omitted.

PAMs

Actuation principles: PAMs can achieve contractile and linear motion by adjusting the gas pressure inside a

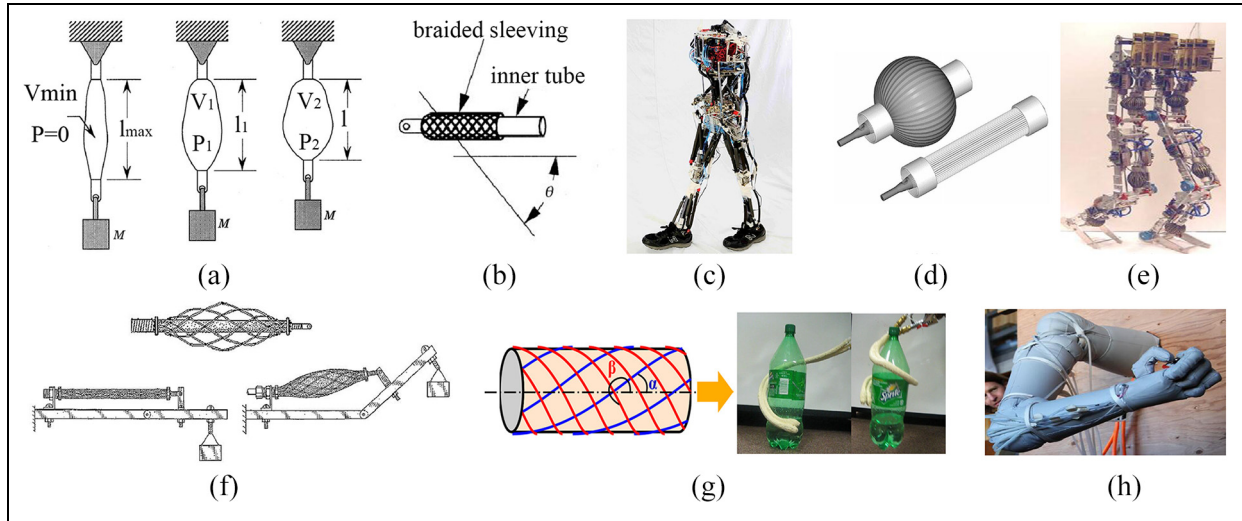


Figure 1. PAMs actuating principles and applications: (a) actuation principle of overpressure PAMs, (b) braided PAM structure, (c) McKibben PAM-actuated biped robot, (d) plated PAM structure, (e) plated PAM-actuated biped robot – Lucy, (f) netted PAM structure, (g) torsional PAM structure and (h) torsional PAM-actuated robot arm.

(a) and (b) Reprinted with permission from an open access article under CC BY licence;²¹ (c) reprinted with permission from Taylor & Francis, Advanced Robotics, Copyright 2018;²² (d) reprinted with permission from an open access article under CC BY licence;²³ (e) reprinted with permission from Springer Nature, Autonomous Robots, Copyright 2005;²⁴ (f) reprinted from US patent;²⁵ (g) reprinted with permission from ASME, Journal of Mechanisms and Robotics, Copyright 2015;²⁶ and (h) reprinted with permission from ASME, Journal of Mechanisms and Robotics, Copyright 2014.²⁷

flexible membrane. PAMs are actuated by the pressure difference between the inside gas and ambient gas, and two actuation methods can be applied: overpressure and underpressure. Usually, PAMs operate at an overpressure: as the membrane is inflated, the PAMs axially contract and exert a force that pulls the load at the end fitting (Figure 1(a)).²¹

Classifications and applications: Based on the tension-carrying structure of the muscle, either embracing the membrane or being embedded in the membrane, PAMs can be classified as embracing types and embedded types. Embracing PAMs can be further subdivided into braided PAMs and plated/netted PAMs based on how the membrane radially expands, by stretching the membrane materials or rearranging the membrane's surface when inflated.

Braided PAMs. Braided PAMs are usually cylindrical in shape and composed of a cylindrical tube or bladder surrounded by a braided sleeving with a constant pitch angle (Figure 1(b)).²¹ The McKibben PAM and sleeved bladder PAM are two basic types of braided muscle, in which the inner bladder is either attached to the end fitting or not attached to the end fitting, respectively.^{28,29} The McKibben PAM is the most extensively applied artificial muscle in anthropomorphic robots with low cost (Figure 1(c)) and can be easily assembled in prostheses and orthotics due to the simple design. Its length-load curves between this type of PAM and biological muscle are similar.^{22,30,31}

Plated PAMs. Plated PAMs have a rearranging-type membrane, which means that the membrane does not stretch when inflated.³² The rearranging-type membrane has numerous pleats in the axial direction, which can expand during inflation and causes the membrane to unfold without material strain (Figure 1(d)).²³ No friction exists, and no energy is required to expand the membrane in the radial direction during the inflation process. Therefore, minimal hysteresis occurs, and a low threshold pressure is required to actuate plated PAMs. Plated PAMs can be applied in accurate and fast positioning devices and compliance actuation robots (Figure 1(e)).^{24,32}

Netted PAMs. Netted PAMs have a surrounding membrane with a low-density network. The low-density network consists of a mesh with relatively large holes and a tightly woven braid. This membrane is also the rearranging type due to the membrane structure. Netted PAMs include the Yarlott PAM, robotic muscle actuator (ROMAC) PAM and Kukolj Muscle.^{25,33,34} A higher force and negligible hysteresis occur due to the absence of friction and membrane stretching. Thus, netted PAMs are usually employed in lifting devices (Figure 1(f)).²⁵

Embedded PAMs. Embedded PAMs have a rubber tube (load-carrying structure) that is embedded in their thin membranes, which can reduce the friction and threshold pressure due to the absence of friction between the rubber tube and the membrane. Embedded PAMs

include the Morin PAM, Baldwin PAM, Paynter knitted PAM and Kleinwächter PAM.^{28,35–37} In addition to linear motion, embedded PAMs, such as the PAM shown in Figure 1(g), can also achieve torsional motion, which can be applied in torsional inflated robots (Figure 1(h)).^{26,27,38}

SMA

Actuation principles: SMAs are metallic alloys that utilise the shape memory effect and can return to their origin shape or size when subject to a memorisation process between two transformation phases. The memorisation process that is applied to actuators is usually thermally or magnetically driven.¹⁹ Typically, SMAs are deformed by an external force and can contract or recover to their original form when subject to stimuli such as heat or a magnetic field.

Classifications and applications: Based on the external stimuli that are applied, SMAs mainly fall into two types of actuators: thermal SMAs (TSMAs) and ferromagnetic SMAs (FSMAs).

TSMAs. TSMAs return to their original shape if heated after deformation, in which the transformation from martensite to austenite has a central role. At low temperatures, a TSMA has a twinned martensite structure, which can be easily deformed by an external force and converted into detwinned martensite. When the TSMA is heated by external or internal heating (Joule heating), it begins to transform from martensite to austenite at the austenite-start (As) temperature and finishes this transformation at the austenite-finish (Af) temperature. The austenitic phase is a highly ordered state, and the TSMA contracts and recovers to the predefined high-temperature shape. Conversely, the TSMA reverts to martensite after cooling, which starts at the martensite-start (Ms) temperature, and is completed at the martensite-finish (Mf) temperature. The TSMA is elongated by the defined external force (Figure 2(a)).^{39–41} Therefore, the shape memory effect is only observed in most TSMAs, when an external stress is applied. This type of SMA is also known as a one-way SMA. In addition, some TSMAs display a two-way shape memory effect, which can act without an external stress.⁴² Nickel–titanium (NiTi) alloys are one of the most extensively applied TSMAs and have been applied to small robots such as fish robots (Figure 2(b)), climbing robots (Figure 2(c)), flying robots (Figure 2(d)) and hand prostheses (Figure 2(e)).^{43–46}

FSMAs. FSMAs demonstrate the shape memory effect in response to a magnetic field, which drives the shape change faster than relatively slow heating and cooling processes. This phenomenon is generated by the

transition among variants of the tetragonal martensite phase that formed during cooling from the cubic austenite phase. In three-dimensional (3D) space, the martensite unit cell has a shorter size along one axis and a longer size along the other two axes than the cubic cell (Figure 2(f)).⁴⁹ The martensite unit cell can be easily, magnetically and mechanically deformed along its shortest axis (Figure 2(g)).⁴⁷ Typically, a predefined force is applied in the short axis direction, which compresses the FSMA; it can return to its original shape when a magnetic field is applied orthogonally to the short axis direction. Due to the fast response and high specific power, FSMAs have also been employed in small-sized robots such as caudal peduncles for fish robots (Figure 2(h)) and flappers for flying robots.^{48,50}

EAPs

Actuation principles: EAPs are smart materials that are capable of producing mechanical deformation in response to electrical stimulation. EAP materials exhibit some features that are beneficial for actuation such as great strain, high power density, versatility, scalability and low cost.⁵¹ These characteristics allow EAPs to emulate biological muscle more closely as ‘artificial muscles’.⁵²

Classifications and applications: According to their activation mechanisms, EAPs can be classified into two major groups: electronic EAPs (e-EAPs) and ionic EAPs (i-EAPs). e-EAPs are activated by electrostatic forces, which exert dimensional changes in response to an electric field. This category includes dielectric elastomer actuators (DEAs) and relaxor ferroelectric polymers (RFPs). i-EAPs are actuated by an electrically induced shift of ions. An electrolyte phase, in which ions are capable of moving, is required for i-EAPs, which is often a liquid. This technology mainly includes conducting polymers (CPs), ionic polymer metal composites (IPMCs) and carbon nanotubes (CNTs).

DEAs. DEAs can generate deformations as a result of electrostatic interactions between two electrodes. DEAs act as capacitors when an external voltage is applied; opposite charges are attracted in the electric field direction, while like charges repulse each other in the direction perpendicular to the electric field. Therefore, the Maxwell stresses exerted in the dielectric materials squeeze the DEAs along the direction of the voltage and expand them in the other two directions (Figure 3(a)). A silicone or acrylic material often acts as the elastomer of a DEA, with a compliant electrode that is applied to achieve large deformation. For this reason, DEAs are extensively applied as actuators for robots: fish robots (Figure 3(b)), flying robots (Figure 3(c)),

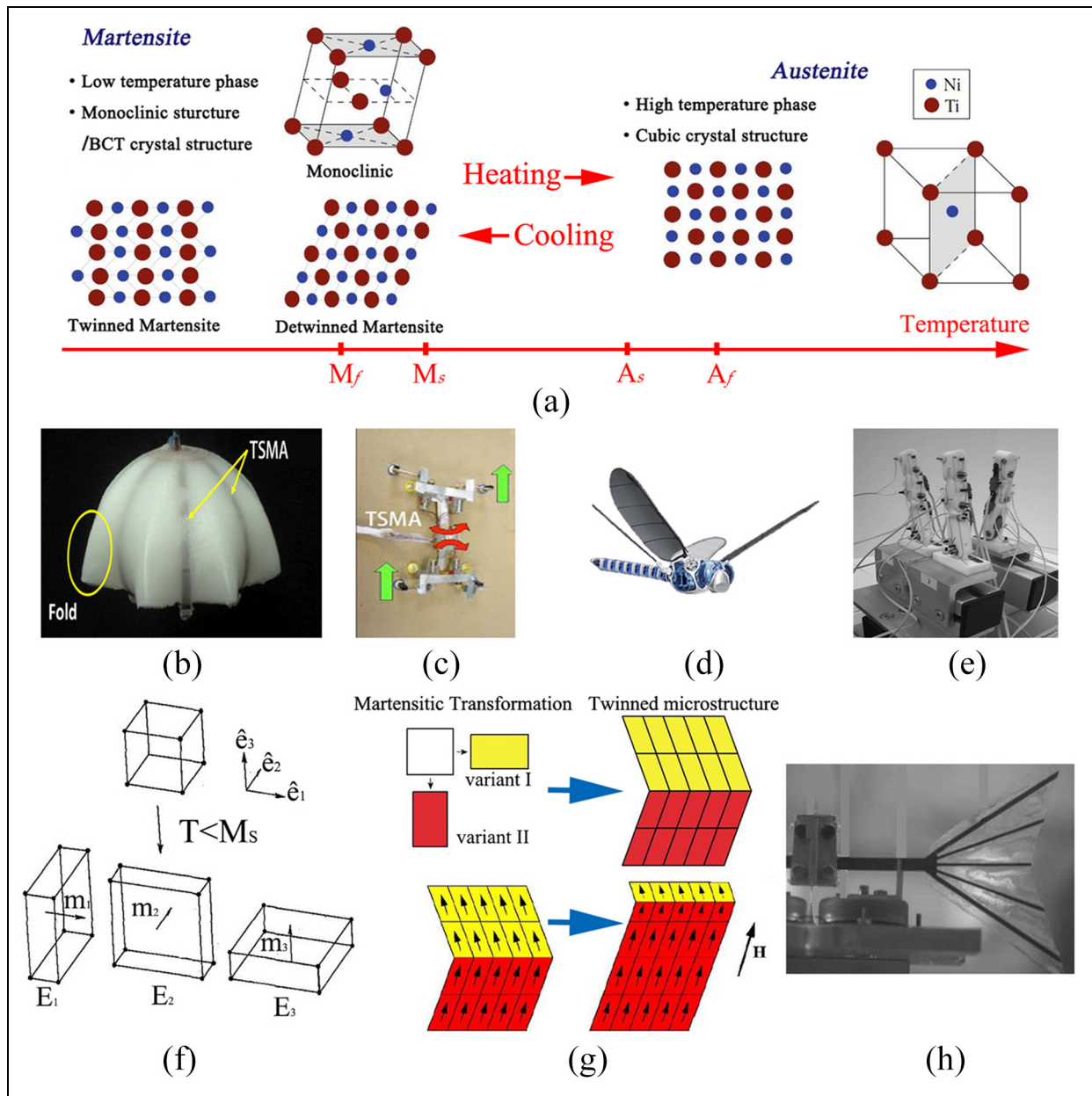


Figure 2. SMAs actuating principles and applications: (a) actuation principle of TSMA, (b) NiTi SMA-actuated jellyfish robot, (c) NiTi SMA-actuated climbing robot, (d) NiTi SMA-steered flying robot, (e) NiTi SMA-actuated hand prosthesis, (f) three kinds of martensitic phases of FSMA, (g) martensitic transformation and twinning of an FSMA and redistribution under a magnetic field in two dimensions and (h) FSMA-actuated fish robot.

(a) Reprinted with permission from Springer Nature, Shape memory alloys: modelling and engineering applications by D.C. Lagoudas, Copyright 2008;⁴¹ (b) reprinted with permission from IOP Science, Bioinspiration and Biomimetics, Copyright 2011;⁴³ (c) reprinted with permission from Springer Nature, RoboCup 2010: Robot Soccer World Cup XIV by M.M. Kheirikhah et al., Copyright 2011;⁴⁴ (d) reprinted with permission from an open access website;⁴⁵ (e) reprinted with permission from IOP Science, Smart Materials and Structures, Copyright 2007;⁴⁶ (f) drawn by the author; (g) reprinted with permission from Elsevier, Materials Science and Engineering: A, Copyright 2004;⁴⁷ and (h) reprinted with permission from Springer Nature, International Journal of Automation and Computing, Copyright 2006.⁴⁸

robot arms (Figure 3(d)) and legged robots (Figure 3(e)–(g)).^{53–60}

RFPs. A ferroelectric polymer material that is often used as an actuator is poly(vinylidene fluoride-trifluoroethylene), abbreviated P(VDF-TrFE). The backbones of

P(VDF-TrFE) are highly polar due to the electronegativity of fluorine. The reversible conformational changes caused by the alignment of polar groups are utilised in actuation.⁵² As shown in Figure 3(h), when an electric field is applied perpendicular to the chain, the ferroelectric that is originally in the nonpolar alpha phase

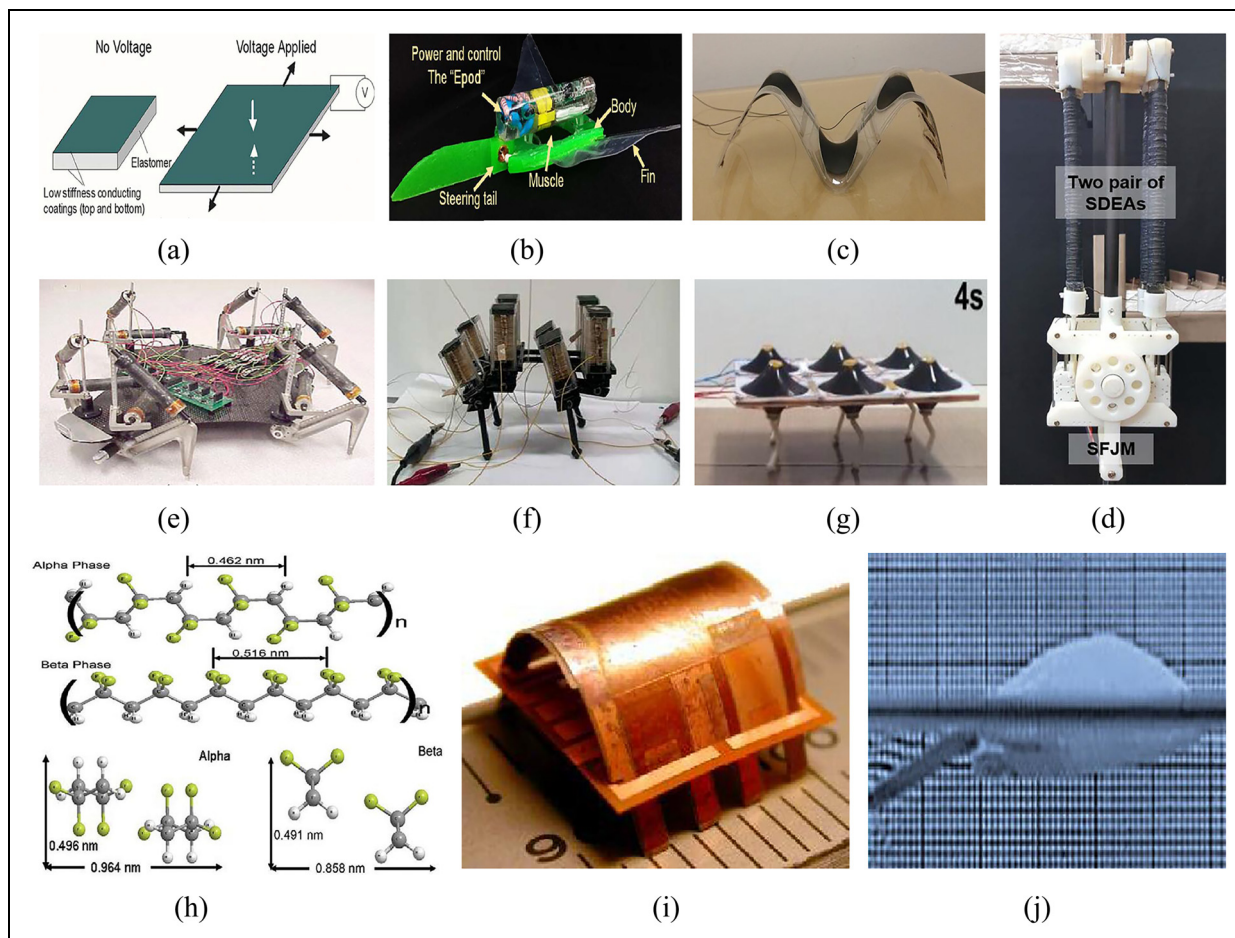


Figure 3. e-EAPs actuating principles and applications: (a) actuation principle of DEAs,⁵³ (b) DEA-actuated fish robot, (c) flapping wings actuated by a DEA for flying robots, (d) DEA-actuated robot arm, (e) DEA-based six-legged robot, (f) DEA-actuated hexapod robot, (g) DEA-actuated quadruped robot, (h) actuation principle of RFPs, (i) RFP-actuated legged robot and (j) RFP-actuated fish robot.

(a), (e) and (h) Reprinted with permission from Elsevier, *Materials Today*, Copyright 2007;⁶¹ (b) reprinted with permission from an open access article under CC BY-NC licence;⁵⁴ (c) reprinted with permission from Springer Nature, *Meccanica*, Copyright 2015;⁵⁵ (d) reprinted with permission from IOP Science, *Smart Materials and Structures*, Copyright 2018;⁵⁶ (f) reprinted with permission from IOP Science, *Smart Materials and Structures*, Copyright 2014;⁵⁸ (g) reprinted with permission from Elsevier, *Sensors and Actuators A: Physical*, Copyright 2017;⁶⁰ and (i) and (j) reprinted with permission from an open access article under CC BY licence.^{62,63}

switches to the polar beta phase.⁶⁴ This switching causes elongation along the chain length and contraction perpendicular to the chain direction. A problem with ferroelectric polymers is the existence of a massive hysteresis and substantial energy dissipation during the actuation process, when a large electric field is applied to reverse the polarisation.⁶⁵ To eliminate the hysteresis behaviour, P(VDF-TrFE) can be irradiated or a small mass fraction of a bulky monomer can be added to disrupt the long-range order to form RFP.^{66,67} Consequently, great reversible electrostriction is obtained in RFPs, which can be applied in millimetre-sized legged robots (Figure 3(i)) and swimming robots (Figure 3(j)).^{62,63}

CPs. CPs are also known as conjugated polymers. The electrochemically changing oxidation state causes

charge addition to or removal from the electrolyte when a voltage is applied to the two electrodes, which is also known as doping. Dimensional changes are caused by electrochemical doping.⁶⁸ As shown in Figure 4(a), the CP expands when it is oxidised as the anions (A-) enter the electrolyte to balance the charge, and the CP contracts when it returns to the reduced state, in which anions have been removed.⁶⁹ The main advantage of CPs over e-EAPs is their low driving voltage, which typically ranges from 1–2 V to 10 V for higher speed and response.⁷⁰ This characteristic combined with high stress renders CPs attractive as actuators. For example, CPs have been applied in rotational motors (Figure 4(b)).⁷¹ In addition, CPs have also been employed to actuate micro-grippers (Figure 4(c)) and fish robots (Figure 4(d)).^{72–75}

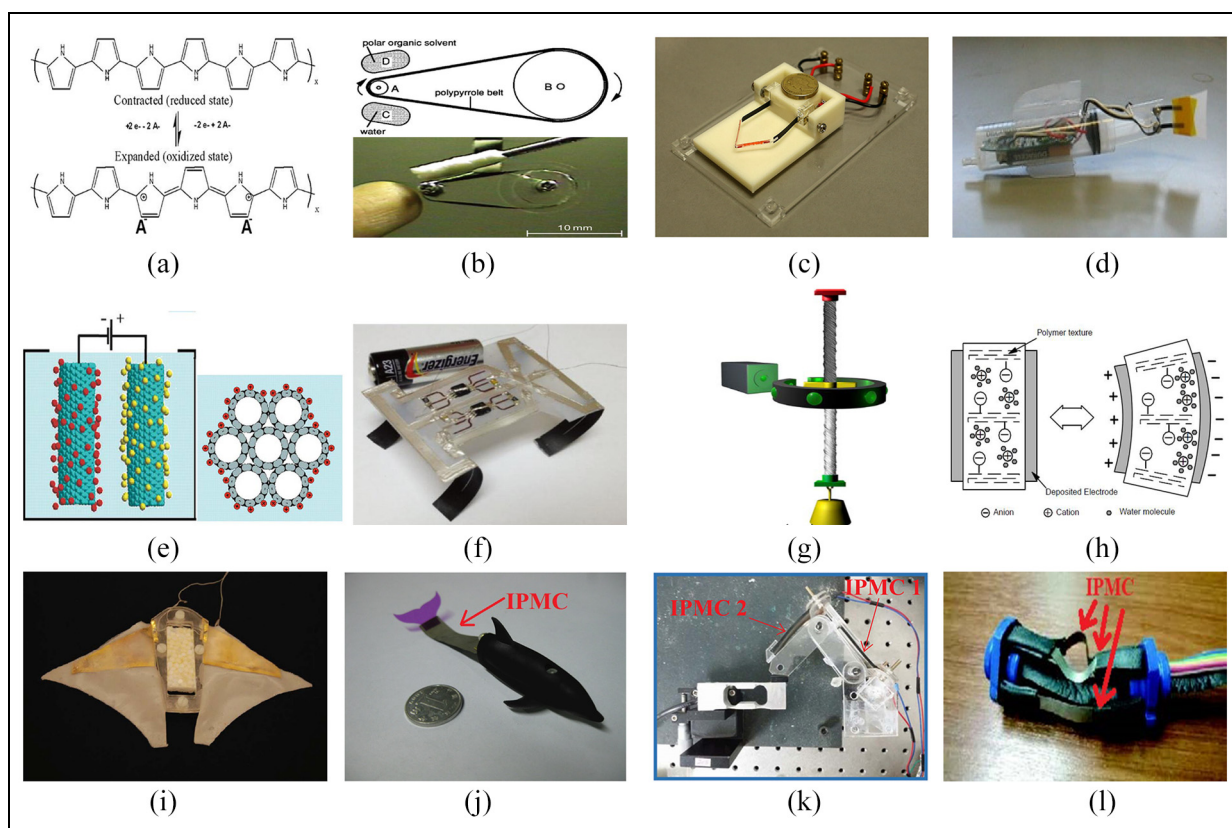


Figure 4. i-EAPs actuating principles and applications: (a) actuation principle of CPs, (b) CP-actuated rotational motor, (c) CP-actuated soft gripper, (d) CP-actuated fish robot, (e) actuation principle of CNTs, (f) CNT-actuated quadruped robot, (g) torsional artificial muscle actuated by CNTs, (h) actuation principle of IPMCs, (i) IPMC-actuated manta ray robot, (j) IPMC-actuated fish robot, (k) IPMC-actuated joint for a robot manipulator and (l) IPMC-actuated joint for a swimming snake robot. (a) Drawn by the author; (b) reprinted with permission from Wiley & Son, *Journal of Applied Polymer Science*, Copyright 1997;⁷¹ (c) reprinted with permission from IOP Science, *Smart Materials and Structures*, Copyright 2015;⁷² (d) reprinted with permission from IOP Science, *Smart Materials and Structures*, Copyright 2009;⁷⁴ (e) reprinted with permission from Elsevier, *Materials Today*, Copyright 2007;⁶¹ (f) reprinted with permission from an open access article under Copyright Taylor and Francis Group, LLC licence;⁷⁶ (g) reprinted with permission from AAAS, *Science*, Copyright 2012;⁷⁷ (h) reprinted with permission from Elsevier, *Sensors and Actuators A: Physical*, Copyright 2003;⁷⁸ (i) reprinted with permission from an open access article under Copyright Taylor and Francis Group, LLC licence;⁷⁹ (j) reprinted with permission from IOP Science, *Smart Materials and Structures*, Copyright 2013;⁸⁰ (k) reprinted with permission from an open access article under CC BY-NC licence;⁸¹ and (l) reprinted with permission from Elsevier, *Materials Today: Proceedings*, Copyright 2016.⁸²

CNTs. A CNT is a single rolled sheet of graphite with a large surface area and high conductivity, whose size is on the micrometre scale. The main cause of actuation is electrostatic forces. As shown in Figure 4(e), CNTs act as electrodes and/or counter electrodes when they are immersed in electrolytes.⁶¹ When a potential is applied, ions are attracted to the nanotubes, which cause charging and rearrangement of the electronic structure. The electrostatic repulsive forces between two charges on the CNT surface can elongate and expand the nanotubes.^{83,84} Typically, actuation is generated in films or yarns that are composed of many nanotubes. For instance, CNT films that are often applied as bending actuators to drive a soft gripper can also be utilised as buckypaper actuators to actuate a centimetre-sized walking robot (Figure 4(f)).^{76,85} CNT yarns perform as artificial muscles that can generate torsional and tensile motion (Figure 4(g)).⁸⁶ In addition

to the electrical method, this type of torsional artificial muscle can be chemically and thermally driven.⁷⁷

IPMCs. An IPMC is composed of a polymer electrolyte sandwiched by two high-surface area metallic electrode layers, and the two electrodes interpenetrate the polymer electrolyte.^{87,88} The polymer electrolytes that are often applied, such as Nafion, are neutralised with certain counterions, which are balanced by the electrical charge of the anions fixed to their backbone.⁸⁷ When an electric field is applied perpendicular to the IPMC layers, the mobile cations in the polyelectrolyte move towards the oppositely charged electrode (Figure 4(h)), which cause swelling at the negative side and shrinkage at the positive side to achieve bending of the entire IPMC actuator.^{78,89} Numerous robotic applications that are based on IPMC actuators have been reported. First, IPMCs can be readily employed as actuators of

soft grippers due to their inherent bending motion.^{90,91} Second, IPMCs are the preliminary technology for hydrodynamic propulsion such as IPMCs in manta ray robots (Figure 4(i)) and fish robots (Figure 4(j)).^{79,80} Finally, IPMCs can perform as robotic joints that move in parallel such as IPMCs in a millimetre-sized manipulator (Figure 4(k)) and a snake robot (Figure 4(l)).^{81,82}

Newly developed actuators

In recent years, various kinds of promising actuators have developed and been employed in robotic applications with different smart materials. Representative actuator technologies, including twisted fibre actuators (TFA), HGA and hydraulically amplified self-healing electrostatic (HASEL) actuators, will be discussed.

TFAs. Actuation principles: high-strength polymer fibres are transformed to artificial muscles by twist insertion. Twisted yarns of polymer fibres can generate linear and torsional actuation after volumetric expansion, which can be achieved via different mechanisms, including thermal expansion and volumetric expansion of absorption. The heat of thermal actuation is generated via two mechanisms: Joule heating and photo-thermal heating.⁹² The absorption actuation employs moisture-sensitive silk fibre to exert deformation while changing the relative humidity.⁹³ The one-end-tethered twisted yarn responds to the structural volumetric change by untwisting at its free end to form the torsional actuator. The two-end-tethered twisted yarn can only change the diameter by translating and contracting in length instead of untwisting in the end, which forms the linear actuator.

A typical feature of this kind of actuator is the twisted fishing line (e.g. nylon 6) or sewing thread (e.g. nylon 6.6). First, this thermally driven artificial muscle can be constructed by inserting an extreme twist into the fibre. Second, the twist is further inserted to form a self-coiled yarn (Figure 5(a)).⁹⁴ Finally, an annealing process is applied to yarn to avoid untwisting after disengaging the fibre end-fixing. The nylon artificial muscle can achieve large output contraction and generate super-high mechanical power. The excellent muscle stroke and work capacity are retentive as the fibre diameter changes by orders of magnitude. This near-invariance of actuation performance indicates great scaling of structure and properties. Therefore, the nylon muscles can be converted to a two-ply (Figure 5(b)) configuration and braided structure (Figure 5(c)).^{94,95} The scalable nylon artificial muscle enables a larger strain and stress output, which is applied in macroscopic applications, such as the light-weight prosthetic hand (Figure 5(d)),⁹⁵ where the fingers are actuated by a twisted nylon artificial muscle and soft

robotics, where two twisted nylon fibres are inserted into the substrate, which is represented by blue lines (Figure 5(e)).⁹⁶

HGAs. Actuation principles: hydrogel polymers with high water contents (≥ 90 wt%) can switch their sizes and shapes by the uptake and release of water to change the water content in the polymer work, and the polymer actuators perform deformation and movement in response to various environmental stimuli (Figure 5(f)).⁹⁷ The main branch of the HGA family consists of pH-responsive hydrogels, which sensitively respond to pH changes in the ambient environment with swelling or shrinking deformation. When experiencing pH variation, the hydrogel polymer backbone will be ionised and the electrostatic repulsion is generated between adjacent polymer chains, which enables the absorption of water and causes hydrogel swelling.^{102,103} Some hydrogel polymer can undergo reversible shifts in morphological and physical phases in response to temperature variations. The underlying mechanism of the thermally driven hydrogel is attributed to a solubility shift in aqueous solution.¹⁰⁴ These two methods are limited by the uncontrollability on/off state of actuation. Thus, a precisely controllable method is introduced. Electric-responsive hydrogel can swell/deswell in an electric field, which is combined of coulombic, electrophoretic and electro-osmotic interactions.^{105,106} Electrical-responsive hydrogels are often employed in an aqueous electrolyte, and the direction migration of mobile ions in the solution occurs in an applied electric field, which causes contraction of the hydrogel. An osmotic pressure difference is then exerted due to the concentration gradient of ions. The hydrogel polymers generate swelling and deswelling according to the osmotic pressure increase and decrease, respectively.

To respond to various stimuli, in this way, the hydrogel-based actuators could perform deformation in various environments. HGAs are soft and wet materials that can interact with the internal constituents of the human body in a safe and human-friendly manner. Therefore, HGAs are raising tremendous attention and showing their potential in applications such as grippers (Figure 5(g)),⁹⁸ artificial muscles (Figure 5(h))⁹⁹ and drug delivery.¹⁰⁷

HASEL actuators. Actuation principles: two types of HASEL actuators achieve linear actuation motion. First, the planar HASEL actuator, which has an elastomeric shell, is partially covered by a pair of opposing electrodes outside and filled with a liquid dielectric inside.¹⁰⁰ An electric field exists through the liquid dielectric when voltage is applied to the electrode. The resulting electrostatic Maxwell stress presses and displaces the liquid dielectric from between the electrodes

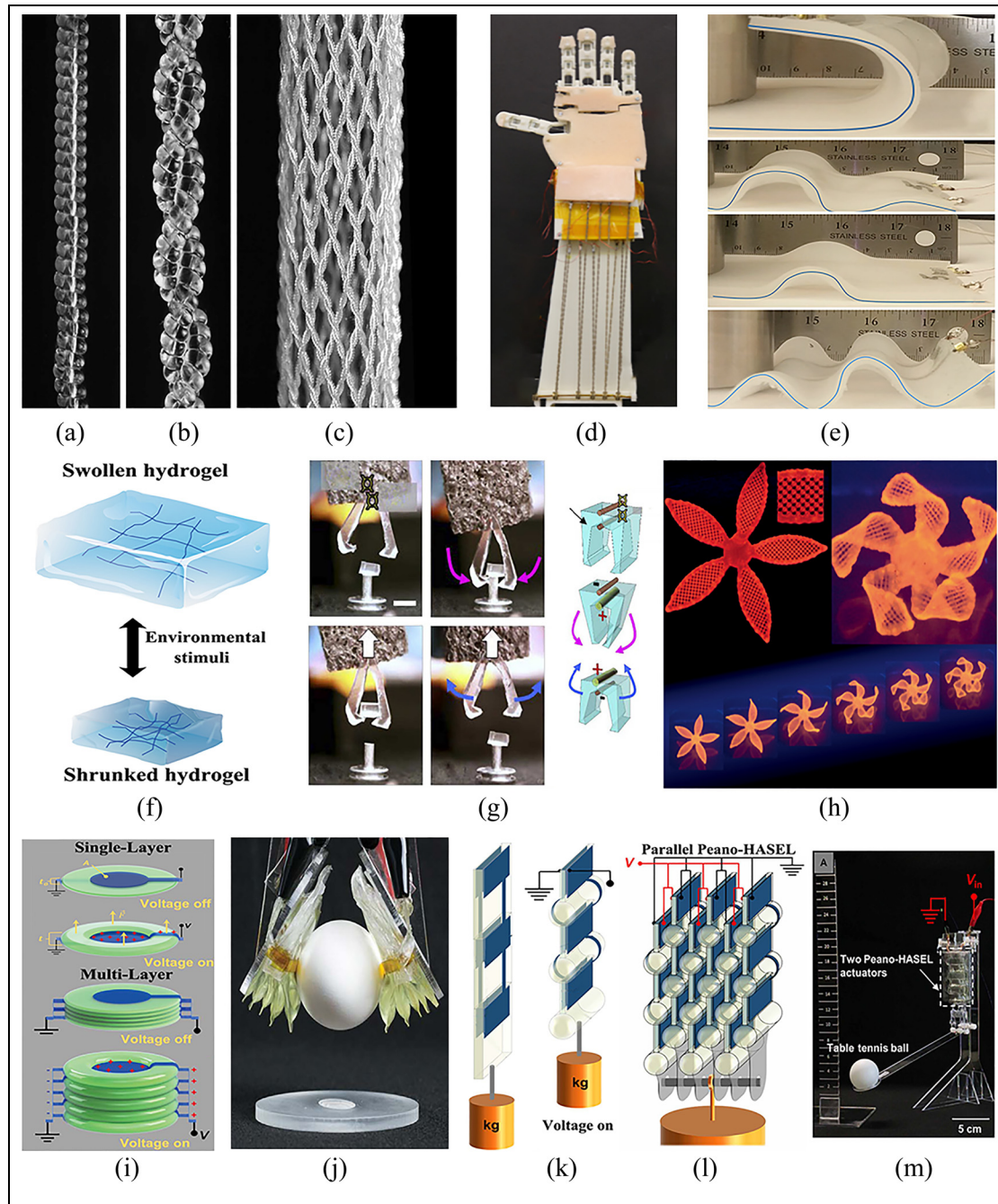


Figure 5. (a) A single twisted coiled nylon fibre, (b) two-ply twisted nylon fibre, (c) braided actuator of twisted nylon, (d) a hand prosthesis actuated by nylon artificial muscle, (e) different geometry of robot made from twisted and coiled nylon polymer, (f) actuation principle of hydrogel, (g) a small size hydrogel gripper; (h) four-dimensional (4D) printed hydrogel actuator driven by temperature, (i) basic structure of planar HASEL actuator, (j) a gripper constructed by multi-layer planar HASEL actuator, (k) basic structure of peano-HASEL actuator, (l) parallel configuration of peano HASEL actuator and (m) a lever arm actuated by peano HASEL.

(a)–(c) Reprinted with permission from AAAS, Science, Copyright 2014;⁹⁴ (d) reprinted with permission from IOP Science, Bioinspiration and Biomimetics, Copyright 2016;⁹⁵ (e) reprinted with permission from Springer Nature, International Journal of Intelligent Robotics and Applications, Copyright 2017;⁹⁶ (f) reprinted with permission from an open access article under CC BY licence;⁹⁷ (g) reprinted with permission from Springer Nature, Nature Communications, Copyright 2013;⁹⁸ (h) reprinted with permission from Springer Nature, Nature Materials, Copyright 2016;⁹⁹ (i) and (j) reprinted with permission from AAAS, Science, Copyright 2018;¹⁰⁰ and (k)–(m) reprinted with permission from AAAS, Science Robotics, Copyright 2018.¹⁰¹

to the surrounding volume. Actuation strain increases with an increase in the input voltage, where the resulting hydraulic pressure causes the soft structure to deform into a toroidal shape and gain an elongation actuation movement, and this type of actuator could be stacked to achieve higher strain and force (Figure 5(i)).¹⁰⁰ Second, a peano-HASEL actuator is constructed with a series of pouches made from a flexible and inextensible shell that is filled with a liquid dielectric. Electrodes cover a portion of each pouch on both side of the actuator. The electrostatic force causes electrodes to progressively close when a voltage is applied. The pressure forces dielectric fluid into an uncovered portion of the pouch, which causes the pouch to transition from a flat cross section towards a circular cross section. This transition causes linear contraction of the actuator as the shell is inextensible (Figure 5(k)).¹⁰¹ Furthermore, the parallel configuration obtained from the peano-HASEL actuator has greatly amplified the output force (Figure 5(l)).¹⁰¹

The HASEL actuator blends soft fluidic actuators with muscle-like performance of DEAs to achieve a variety of actuation modes without rigid frames or pre-stretched mechanisms. The hydraulic principles enable HASEL actuators to scale actuation output strain and force. The scalability gives HASEL actuators the capability to construct a soft gripper that can handle delicate objects (Figure 5(j))¹⁰⁰ and an artificial muscle that can lift more than 200 times their weight (Figure 5(m)).¹⁰¹ Unlike traditional solid DEAs, which would be permanently damaged due to a high electric field, the use of a liquid dielectric enables HASEL actuators to self-heal from a dielectric breakdown. The self-healing property improves the durability and stability of HASEL actuators, which demonstrates promise for applications in robotics.

Results

This study selected typical actuators that represent each type of artificial actuator technology. We collected parameters of these typical actuators, including their strain, stress, strain rate, work density, specific power and efficiency. First, this section successively compares typical actuators that are based on single actuation parameters, which demonstrates the superior actuators for each actuation property. These comparisons can serve as references in actuator selection to satisfy certain actuation parameter requirements. Second, this section simultaneously compares the six actuation parameters of the typical actuators with those of biological muscle to obtain insights into each type of actuator. The merits and insufficiencies of each typical actuator are given, and improvement methods and new ideas are proposed based on the comparison results.

Actuation parameters of representative actuators

This study reviewed the actuation parameters of skeletal muscle, the McKibben PAM, NiTi-based SMA, acrylic-based DEA, P(VDF-TrFE)-based RFP, polypyrrole (PPy)-based CP, CNT-based actuator, Nafion-based IPMC, nylon TFA, poly(vinyl alcohol)-based HGA and liquid dielectrics-based HASEL. These actuators are the most prevalent among each type of technology and act as samples to assess the actuation capacities of these classifications. The actuation performances of the biological and artificial muscles based on the six key parameters are listed in Table 1, where the maximum values of the actuation parameters are given. Although some of the maximum values were obtained from theoretical models or ideal materials, they demonstrate the potential upper limit for each actuator

Table 1. Actuation performances of biological and artificial muscles.

Actuators	Parameters						References
	Strain (%)	Stress (MPa)	Strain rate (%/s)	Work density (kJ/m ³)	Specific power (kW/kg)	Efficiency (%)	
Biological muscle	40	0.35	50	40	0.28	40	108 and 109
PAM	25	1.16	800	200	10	49	18, 32, 38, 110 and 111
SMA	10	200	300	10000	50	10	108 and 112–115
DEA	380	7.7	450	3400	3.6	80	53, 65, and 116–118
RFP	7	45	2000	1000	4	80	66, 67, and 119–122
CP	10	34	12	100	0.15	1	123–127
CNT	3	26	19	1000	0.27	0.55	65, 77, and 128–131
IPMC	40	3	3.3	5.5	0.00256	1.5	88, 132, and 133
TFA	49	22	50	5.3	5.3	2	92 and 94
HGA	20	0.005	2	460	0.0002	0.2	134–137
HASEL	170	0.3	2176	64.4	0.6	21	100 and 138

PAM: pneumatic artificial muscles; SMA: shape memory alloys; DEA: dielectric elastomer actuators; RFP: relaxor ferroelectric polymers; CP: conducting polymers; CNT: carbon nanotubes; IPMC: ionic polymer metal composites; TFA: twisted fibre actuators; HGA: hydrogel actuators; HASEL: hydraulically amplified self-healing electrostatic actuators.

technology, which could guide the future development trends of robotic actuators.

Single parameter comparison

To evaluate these actuators for various purposes or different applications, single actuation parameters were compared according to the collected data.

1. Strain is expressed as the ratio of total deformation to the initial dimension of the material

body along the direction in which actuation is being applied; it reflects the deformability of actuator materials. As shown in Figure 6(a), due to the low modulus and high dielectric strength of the acrylic elastomer of the DEA and special structure of HASEL, giant strains of 380% and 170%, respectively, are achieved at high applied fields.^{100,139} The PAM and IPMC also exhibit relatively large strains that approximate the strain of biological muscle (20%–40%)

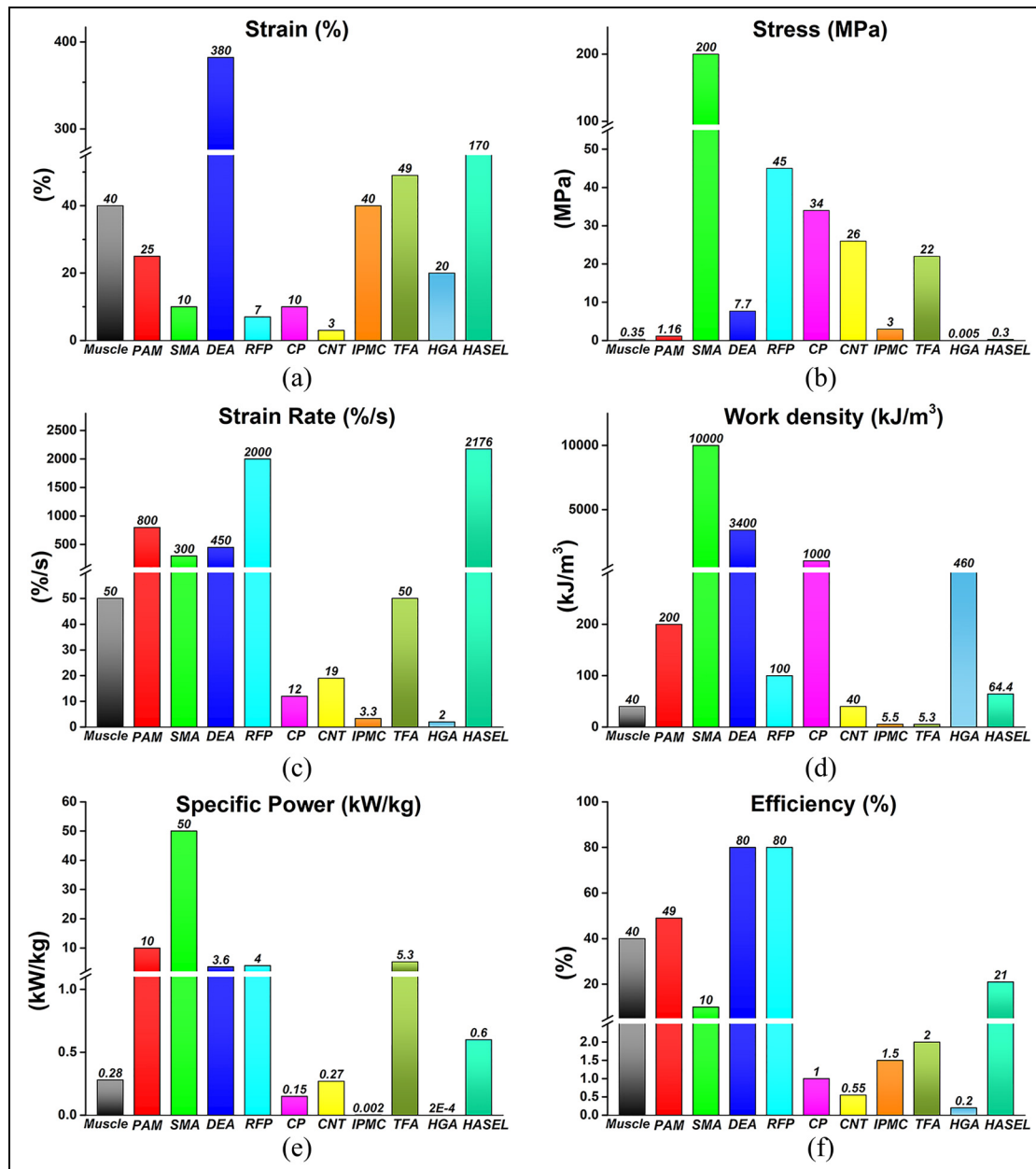


Figure 6. Single actuation parameter comparisons between biological and artificial muscles, wherein the breaks on the vertical axes and in the bars indicate that the values above the break are higher by at least an order of magnitude than the values below (data are all from Table I). (a) Strain comparison, (b) stress comparison, (c) strain rate comparison, (d) work density comparison, (e) specific power comparison, and (f) efficiency comparison.

due to their soft bladder or electrodes. The strains of the other actuators are less than 10%.

2. Stress is expressed as the ratio of the output force to the cross-sectional area normal to the actuation direction. The output force scales linearly with the cross-sectional area for all actuator materials, which implies that higher stress causes higher output force when actuators have the same size. In Figure 6(b), the SMA shows ultra-high stress to 200 MPa, and the RFP, CP and CNT also exhibit relatively high stresses. High output stresses are rooted in their high elastic moduli (>1 GPa), while materials with relatively low elastic moduli have low output stresses such as the PAM, DEA and IPMC.
3. The strain rate is the change in strain per unit time and indicates how fast the material can expand or shrink in response to the motion commands delivered from the central controller. Thus, a high strain rate is essential for materials or actuators when applied to robots with a high actuation bandwidth. In Figure 6(c), the e-EAPs, that is, the DEA and RFP, exhibit overwhelming superiority due to their high dielectric constants. The HASEL actuator is actuated by the mechanism of DEA and achieves a high strain rate accordingly. The PAM and SMA also display high strain rates due to pneumatically and electrical-heating-driven methods. However, ion diffusion and the transport velocity limit the strain rate of the i-EAPs, including the CP, CNT and IPMC.
4. Work density is the work that is generated in the actuator per cycle and normalised by the volume. This parameter indicates the amount of work that can be exerted by the actuator in a limited space. As shown in Figure 6(d), the SMA, DEA and CP present higher work densities than the other types of actuators. Actuators with a high work density are marked by either a large actuation strain or a high output stress.
5. Specific power is the ratio of the power that is generated by the actuator to its mass. With an increasing emphasis on the light weight and miniaturisation of working devices, a lower mass and a higher power are required. With a high work density and high strain rate, the PAM, SMA, DEA and RFP demonstrate high specific power, as shown in Figure 6(e). In addition, i-EAPs are still constrained by the low strain rates, which generate low specific power.
6. Efficiency corresponds to the ability of actuators to convert the input energy to output mechanical energy. This parameter determines the power supply volume and continuous working period

when the actuator is applied in robotics. In Figure 6(f), electrically driven actuators, such as the DEA and RFP, show very high efficiencies to 80%. The PAM demonstrates an actuation efficiency that is similar to that of biological muscle, while the SMA has only a 10% efficiency due to heat dissipation. The efficiencies of the i-EAPs do not exceed 1% due to their low electromechanical coupling.

Artificial actuators have better performances than biological muscle from the aspect of single actuation parameters. However, the comprehensive actuation performances of these actuators compared with biological muscle remain unclear, and further discussion is needed.

Comprehensive actuation performance comparison

To understand the benefits and drawbacks of each type of actuator, the comprehensive actuation performances are analysed in this section. Artificial actuator technologies are individually compared with biological muscle to evaluate their actuation advantages and challenges.

PAMs. Of all the PAM technologies, the McKibben PAM is the most prevalent due to its low cost and simple and compact structure. This muscle is constructed with an elastic inner tube surrounded by an expandable braided sleeve. The braided sleeve translates the volumetric increase in the inner bladder to axial contraction, which is capable of generating a pulling force. The length and diameter of the braid change as the pitch angle changes. The muscle would contract until a pitch angle of 54.7° is attained,³⁸ which is the critical angle that corresponds to the maximum volume of the inner bladder and a zero contract force, and the muscle would stretch until the pitch angle decreases to its lower limit, which significantly depends on the braided fibre thickness and strand density. However, the tension force that is generated during contraction depends on the muscle diameter and pitch angle at rest, as well as the driving air pressure. The generated force decreases greatly with an increase in the initial angle to the critical angle and then the muscle produces negative forces.¹⁴⁰ Consequently, the range of contraction–extension (i.e. strain) and tension force (i.e. stress) is determined by the muscle size, woven pattern and driving pressure. As shown in Figure 7(a), the strain and stress of this PAM are slightly higher than those of biological muscle. The strain of the McKibben PAM is typically 25% in practice, and a 1.16 MPa output stress is achieved at an input air pressure of 5 bar.^{18,38} Based on the output strain, output stress and ease of assembly, McKibben PAMs can be extensively applied in task-based robot

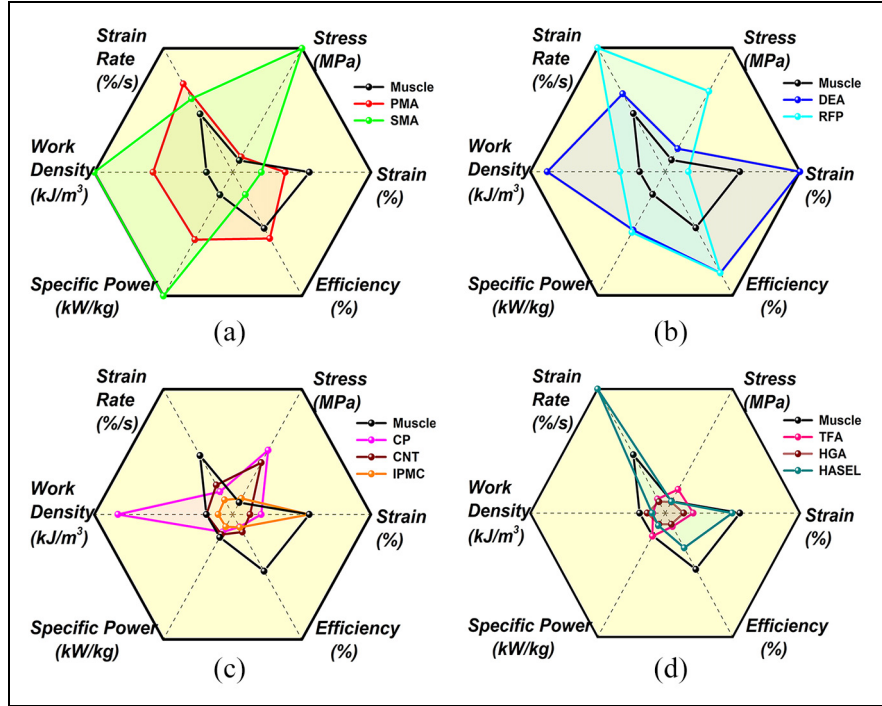


Figure 7. Comparisons of the comprehensive actuation performances between different artificial actuators and biological skeletal muscle. In these radar charts, each corner represents an actuation parameter. The centre of the radar figure represents the value of zero, while the boundaries of the radar chart represent the theoretical maximum value of reviewed actuator technologies, which is listed in parentheses. (a) Comparison between PAM, SMA and skeletal muscle; (b) comparison between e-EAPs and skeletal muscle; (c) comparison between i-EAPs and skeletal muscle; and (d) comparison between newly developed actuators and skeletal muscle.

hands and arms such as the Festo Bionic Soft Hand, Shadow Biomorphing Arm, Festo Airic's Arm and 7 degrees of freedom (7 DOF) robot arm developed by B. Tondur.^{141–144}

The most remarkable advantage of the McKibben PAM is its high specific power, which is derived from the light weight of the actuator materials and compressed air, which is typically in the range of 0.5–2 kW/kg to a maximum of 10 kW/kg.^{110–112} The work density is approximately 0.2 MJ/m³.³⁸ With the relatively fast strain rate of approximately 800%/s, the McKibben PAM performs better in these aspects than biological skeletal muscle, and thus, is suitable for biped walking robots, humanoid robots and Kangaroo jumping robots,^{22,145,146} where high power actuators are required. The McKibben PAM's energy efficiency is approximately 0.32–0.49; the energy efficiency of human muscle is 0.4.^{38,112}

Despite the distinct positives, the McKibben PAM shows nonlinear strain-stress features, which are caused by viscoelastic properties of inner tube materials, the compressibility of air and complex behaviour of the braided configuration. The nonlinearity in combination with inherent dry friction between the sleeving strands and the inner tube causes actuation hysteresis, which increases the complexity of their model and control.

Thereby, the McKibben PAM is not suitable for application to the scenario in which accurate positioning is required. The required compressor in the conventional McKibben PAM makes the pneumatic system heavy, bulky and unsuitable for use as a micro-actuator, where compact and weight minimisation configurations are desired.

SMAs. The NiTi SMA provides significant displacement as a hard material; the most prevalent method for manufacturing SMA is vacuum melting, where NiTi alloys are melted by vacuum induction melting in a graphite crucible, where the carbon content increases and TiC is mixed in the alloy.¹⁴⁷ In addition, SMA can be produced by many other ways such as the heat treating method, powder metallurgy method and thermal spray method.¹⁴⁸ The strain is typically 5%, with a maximum value of 10%.^{108,112,113} This SMA exerts a large force per unit area of more than 200 MPa. Therefore, NiTi SMA is extensively employed as a micro-actuator or artificial muscle in robotics. The SMA reacts directly to an external stimulus, which significantly reduces the actuator's complexity and size. Thus, the NiTi SMA has a very high work density of 10 MJ/m³, which is 25 times that of DC motors, and an unmatched specific power of 50 kW/kg, which means that it can lift 100

times its weight.^{112,113} As shown in Figure 7(a), the stress, work density and specific power of this SMA are the highest among all the actuators. Furthermore, the NiTi SMA can act in a fully 3D manner, which allows the actuator to extend, bend and twist, separately or simultaneously. These excellent characteristics have enabled application of the NiTi SMA in micro-walking robots, climbing robots, flying robots, jumping robots, swimming robots and hand prostheses.^{43–46,149,150}

The main challenge is the low response time and low operational frequency of the NiTi SMA, which stem from a relative high heat capacity and density of the material. These disadvantages caused difficulties in the rapid transfer of heat from active elements. The response time of the NiTi SMA can be reduced to several milliseconds, with a maximum strain rate of 300%/s, when a very large electrical current is used for heating.¹¹⁴ However, the relatively slow cooling process still limits the actuation cycle time, even with an active or passive cooling method. The response time is also affected by the size and shape: the smaller diameter actuator heats faster due to higher resistivity and cools faster due to a higher surface-to-volume ratio. Another challenge is the low efficiency, which is approximately 10% theoretically and usually less than 5%, in practice; these values are much lower than the efficiency of biological muscle (Figure 7(a)).^{108,115} Most SMA actuators are based on a spring configuration but the stress distribution is not constant over the spring cross section, which require a larger volume of material to be heated or cooled for the same output force and further reduces the actuator's efficiency. For optimal use of the NiTi SMA, a straight wire configuration is recommended due to a greater amount of work generated from less material volume.

e-EAPs

DEAs. Among the e-EAPs, the acrylic very high bond (VHB) elastomer-based DEA is discussed due to its soft material properties, which allow high strain and stress. The DEA manufacturing process can be subdivided into two stages. First, the coating stage: the coating will be applied to a layer of mixture with a controlled thickness on moulds with the desirable configurations, which are fabricated using lithography. A metal electrode will be applied to the corrugated side of the elastomer film. Second, the assembly stage: the laminated DE films are stacked or rolled to form the actuator.¹⁵¹ High strains to 380% are achieved by the VHB elastomer materials when high electric fields are applied. However, such large deformation cannot be attained with simple linear configuration actuators. Topologies of actuators, such as stack or conical topologies, are applied to achieve large displacements, which typically range from 10% to 100%.^{53,139,152} The stress

of VHB elastomer is 7.7 MPa at a high voltage;^{53,114} however, high-stress output is challenging with a simple film structure. Most DEAs utilise lateral expansion for force output; thus, the output stress can be amplified by stacking or rolling the dielectric elastomer and can be enlarged using them in bundles. As shown in Figure 7(b), the strain surpasses that of biological muscle, and the output stress is also higher. This type of DEA has been applied as an actuator for a hexapod robot and even for an arm-wrestling robot that can compete with a human.^{118,153} The high strain and stress produces a high work density of 3.4 MJ/m³ and a high specific power of 3.6 kW/kg.^{53,65,114,115} The strain rate of DEAs is 450%/s due to the charges' quick response to an electric field. Furthermore, due to its simplicity and low modulus, this DEA is suitable for applications where mechanical compliancy and compact sizes are essential. Thus, DEAs have also been employed as flapping wings in flying robots, where a high actuation frequency is essential.¹¹⁸ The actuation efficiency ranges from 60% to 80%; this high efficiency is primarily attributed to the direct transformation from electric energy to mechanical energy.^{114,115}

However, the high voltage used to drive the DEA is unacceptable in various applications and enforces an external electric source.^{154,155} A large dielectric constant that corresponds to a greater capacitance is desired, which reduces the actuation electric field. Therefore, components, such as organic dipole molecules, high permittivity ceramic fillers or conductive nanofillers, are incorporated in the DEA to improve the dielectric constant. However, these methods often cause side effects such as decreased dielectric strength, reduced energy density or stiffening and agglomeration.^{156–158}

The electromechanical instability is the second challenge for the DEA. The Maxwell stress exerted by the DEA is above a certain threshold and triggers a feedback loop of film compression until it breaks down, which causes failure of the actuator. Therefore, a rigid prestretch structure is essential for the DEA to maintain tension and surpass the threshold.¹³⁹ However, the prestretch mechanism produces an additional load, which reduces the DEA work density and specific power. A stress concentration occurs at the interface between the rigid frame and the soft elastomer material.

The third obstacle is that the compliant electrodes are required for the DEA. The DEA's electrodes must be more compliant and stretchable than elastomer film to prevent a stiffness constrain. In addition, the durability and reliability of electrodes should be considered; electrodes have to maintain conductivity across several millions of actuation cycles with large deformation.

RFPs. The RFP based on P(VDF-TrFE) has a phase transition between ferroelectric transition and paraelectric transition with an increase in temperature. In the

ferroelectric phase, a reversible molecular change between the nonpolar form and the polar form can exert polarisation change; this characteristic leads to output strain and high stress. Poly(vinylidene fluoride) (PVDF)-based actuators are usually fabricated via the layers that formed by gluing two PVDF sheets together; the layers were clamped to a substrate with their polarisations in opposite directions.¹⁵⁹ Recently, the electric poling-assisted additive manufacturing (AM) process, which combines AM and polymeric poling process, has been introduced to PVDF-based actuators.¹⁶⁰ The maximum strain of contraction perpendicular to the electric field can be 7% in low-frequency driving fields.⁶⁸ Therefore, RFPs have been applied in millimetre-sized legged robots and fish robots.^{62,63} Except for the low strain values, the RFP actuation parameters transcend those of biological muscle (Figure 7(b)), with an output stress of 20 MPa during contraction and 45 MPa during the isometric state.^{66,116,117} Furthermore, the field-induced deformation in high-elastic-modulus RFP can be operated at high frequency, which yields a strain rate of 2000%/s, a high work density of 1 MJ/m³, a high specific power of 4 kW/kg and a maximum efficiency of 80%.^{66,118,119,161} The configuration of the RFP actuator is designed to be a single layer or multi-layer structure as the strain output at high frequency is smaller than that at low frequency.

For RFP actuators, the difficulty stems from the high level of driving field, which is close to the dielectric breakdown point.¹⁵⁵ The low sensitivity to the external stimulus limits the performance of the actuator and a large portion of the input energy will be extracted to match the load rather than act as an output force, which reduces the efficiency of the actuation system.¹⁵⁸ In addition, the ferroelectric–paraelectric transition occurs over a narrow range and involves a large hysteresis, which prevents an enhanced response from practical and general applications.

i-EAPs

CPs. CPs based on PPy are outstanding in this class due to their capability of producing more significant strain and stress, which are commonly employed as actuators. The oxidation/reduction reactions, which induce anionic dopants in PPy exchange for charge balance can produce electrochemomechanical deformation. The PPy-based actuator is fabricated using a two-step method. First, the substrate was coated with a PPy layer, which acts as the seed layer in the electrochemical deposition step. Second, the electrochemical deposition was accomplished by polymerizing the pyrrole monomer via electrochemical oxidation.¹⁶² The strain produced by CPs is 2%–10%, and the maximum stress that is exerted is 34 MPa, even when actuated by a low voltage of approximately 2 V.^{163–165} The PPy actuator

devices can transfer electrical energy to macroscopic mechanical movements and mechanical work via the electrochemical reactions in polymer films. A bilayer or bimorph structure is employed to construct a bending PPy actuator, which includes a PPy layer and a passive layer. Macroscopic bending is caused by electrochemically driven length variations in the PPy film, which produces a stress gradient across the interface of the two films. In addition, the linear actuator is usually formed by a freestanding PPy film or yarns. To produce larger volume and length changes, other linear actuator configurations, such as multi-layered laminated films, folded films, bundles of films and roll-up structure, exist.^{166–169} A work density of 100 kJ/m³ and a specific power of 150 W/kg can be realised in PPy-based CPs due to their high tensile strength and high stiffness.^{122,124} These characteristics render CPs suitable as actuators in grippers and robots.^{72–75}

The selection of counterions and the design of structure have been two main topics: while electrochemomechanical deformation is limited by the counterions dopant, the structure of the actuator determines the robustness and actuation efficiency. However, the output strain of PPy actuators is small as small dopants are employed as counterions, even though the enhanced output strain has been gained by replacing these small counterions with larger counterions. A bilayer PPy actuator requires liquid electrolyte media and a metallic electrode to allow current flow, which increases the complexity and weight of the actuator. A major fraction of input electrical energy is wasted to produce the solvent discharge, which causes a low actuation efficiency. Moreover, these reactions cause pH variations and new chemicals, which promote the progressive deterioration of the actuation film and reduce the robustness of the actuator.

CNTs. CNT actuators are mainly powered electrochemically, where an electrical field causes swelling or contraction of the CNT when the mobile ions of solvent enter or leave the polymer. CNT actuators are explored in the form of sheets or films that act as bending actuators such as buckypaper actuators.^{77,86} The CNT is mainly prepared by the arc-discharged method, where the CNT is synthesised on the electrode when running a DC current of 200 A at 20 V.¹⁷⁰ Other methods, such as the laser ablation method, chemical vapour deposition method, vapour-phase growth method and flame synthesis method, are employed to fabricate the CNTs.^{147,171–173} These actuators demonstrate relatively small strains between 0.1% and 3%.^{86,126,174} A process for continuous production of CNT yarn fabrication was introduced, which enables the CNT yarn to be drawn from a multi-wall CNT forest. Compared with the form of sheet or film, the CNT yarn could be twisted, bent and knotted without structural failure.

Tensile CNT actuators could be constructed by twisted spun yarns or coiled yarns, and the output strains could be improved.^{130,175} However, torsional CNT actuators could be formed by twist spun yarns, with two ends tethered.^{176,177} Typically, the stress output of single-walled CNTs (SWNTs) is approximately 0.75 MPa, and the maximum observed isometric actuator stress of SWNT actuators is currently 26 MPa.¹²⁸ Due to their high elastic moduli and giant tensile strength, CNTs have achieved a work density of 1 MJ/m³ and a specific power of 270 W/kg.^{127,128} These twisted and coiled yarns could be further processed into textiles by weaving and braiding, which could provide a larger tensile contraction and output force.¹⁷⁸ The CNT yarns of these actuators could also be driven electrothermally. Tensile or torsional actuation is achieved by a volume change of the yarn. To accommodate volume changes, guest materials, such as lie wax, are introduced to CNTs and transform a large guest expansion to a yarn expansion.

However, an electrolyte or guest material adds more volume and weight to the actuator system, which reduces the work density and specific power values. Moreover, the small strains of CNTs require some mechanical amplification. For twisted or coiled CNT actuators, small or even no space exists between neighbouring turns, and pre-strain mechanisms are essential due to the lack of space for an actuator to contract. These structures further increase the volume or weight of actuators. In addition, due to poor electromechanical coupling, CNT actuators require substantial energy recovery to achieve reasonable efficiencies. The bandwidths of these actuators are low due to the ion exchanging speed, which limits the strain rate.¹⁷⁹ Electrochemical driven CNT actuators rely on electrolytes to exchange ions, even though in some applications the liquid electrolytes are substituted. For example, a textile CNT actuator was driven with an ionically conducting gel instead of liquid electrolyte.

IPMCs. Manufacturing an IPMC actuator starts with the core part, an ionic polymer membrane and two conductive electrodes on both sides. Generally, IPMC manufacturing is divided into four steps: first, pretreatment (surface roughening); second, the initial compositing process, including impregnation-reduction and reductant permeation; third, the surface electroding process, including physical deposition and electroplating; and fourth, the ion exchange.¹⁸⁰ The major role of ionic polymers is to store the ions in the ion sites and maintain the required mobility for counterions across the membrane. Furthermore, ionic polymers provide the mechanical stress and force required for the soft IPMC actuators. While numerous polymers have been synthesised to achieve high performance, Nafion holds a place of prominence in the field due to its high proton

conductivity and excellent mechanical properties. Nafion can be easily formed in any desired shape by casting or evaporating methods.^{181,182} IPMCs based on Nafion can generate a large strain to 40%, with a stress of 3 MPa, under a voltage of less than 7 V due to their mechanical response. This large strain enables close emulation of natural muscle. IPMC actuators could use water as a solvent when DC voltage is applied. The success of these actuators in aqueous environments is a major advantage for the extensive use of IPMC actuators in various underwater robots.^{183,184} IPMCs also have self-contained encapsulated electrolytes, which means that they can operate in dry conditions. Commonly, the IPMC actuator is developed using a thin Nafion film. Two polymer films are bonded to the IPMC actuator in a layered manner. Thus, bending is the basic motion of IPMCs, which is usually employed to form the cantilever actuator. Some linear actuators are developed based on IPMC actuators, where many basic units are connected in parallel or series, and utilise the buckles of IPMCs to achieve linear motion.¹⁸⁵ Therefore, IPMCs are extensively applied in robotic applications, such as micro-grippers and even micro-biped and small quadruped robots.^{132,186} The work density is approximately 5.5 kJ/m³, while the specific power is typically 2.56 W/kg.¹⁸⁷

When the IPMC actuator is applied in water, a corresponding increase in deformation beyond the initial state exists after recovering from the actuation stimulus. This phenomenon is referred to as the relaxation effect of IPMC, which causes serious instability of actuators. Although the use of ionic liquids instead of water as the solvent can relieve relaxation, the respond speed will decrease. Controlling the water content could eliminate relaxation but a slight variation in the water content will cause great difference in performance. Furthermore, due to the thickness of Nafion, which is nearly 180 μ m, the output force is low. Apparently, an effective way to improve the output force is to fabricate IPMC with a thicker base membrane. Two methods are available to increase the thickness of Nafion film: multi-layer integration by hot pressing and solution casting.^{181,182} However, the multi-layers are easily separated by long-term use, while the casting method will decrease the output strain and response rate.

As shown in Figure 7(c), the strain, stress, work density and specific power parameters are similar to those of biological muscle, and some of them even have values that are higher than the values for natural muscle. However, the strain rates of i-EAPs are less than 20%/s, even with a high applied voltage or closely spaced electrodes.^{70,124} These slow actuation rates are produced by the slow transport of ions in electrolytes. Furthermore, the actuation efficiencies of i-EAPs are less than 1.5% due to their low electromechanical coupling.^{77,88}

Newly developed actuators. The newly developed actuators combine the strengths of different technologies to address many of the issues in actuators. As shown in Figure 7(d), these actuators achieve qualified actuation performances using different principles to linearly contract applications in a biological muscle-like fashion.

TFA. Twisted yarns of nano/microfibers, such as nylon, polyethylene, graphene and silk, can convert the volumetric expansion form to linear or torsional actuation. Among these twisted fibres, the inexpensive nylon polymer and fibre polymer chains in non-crystalline regions are less and have anisotropic thermal expansion behaviours, which enable relatively large linear actuation (to 49%) when heated. A single twisted nylon actuator is able to withstand loads that are more than 100 times heavier than human muscle with the same length and weight, which causes output stress of 22 MPa and specific work of 5.3 kW/kg. The maximum mechanical work during contraction is 2.17 kJ/m³. The bending and multi-directional motion can be achieved in twisted artificial muscle, which is fabricated via roller-pressing highly oriented nylon filament into rectangular or square cross-sectional beams.⁹² Furthermore, textile construction is extensively employed as an amplifier of twisted actuators, where weaving and knitting are the two main textile processing methods.¹⁸⁸ Weaving has two perpendicular and individual tread systems – warp threads and weft threads – which could scale up force by parallel assembly of single twisted yarns. Knitting keeps the yarns together by loops that give latent potential for being easily deformable, which amplify the output strain by stretchable patterns. Textile processing permits the twisted yarn to build macroscopic actuation units and enables the potential to design more advanced architecture.

The challenge in developing a high-performance actuator is that actuation rates are limited by thermal transport times to access yarn volume. Usually, an electrical heating element involves helically wrapping the twisted muscle for fast heating but passive cooling still constrains the actuation rate. Even though a passive cooling method is immersed in the twisted muscle in water, which enables electrothermal actuation at 5 Hz to produce ~10% stroke, this method could only be employed in special environments.⁹⁴ Second, the maximum energy conversion efficiency during contraction is 1.08% for nylon twisted fibre, which needs to be improved.⁹⁴

HGA. The maximum swelling ratio of some hydrogel materials in deionised water is 8;¹⁸⁹ however, these materials have isotropic structures, and only homogeneous deformation can be achieved with uniform stimuli. For the actuator constructed with hydrogel,

complex movements are essential. The preparation of internal anisotropic hydrogels has become more important for achieving complex deformation. Four main configurations, including the bilayer structure, gradient structure, patterned structure and oriented structure, are employed to build anisotropic actuators.¹³⁴ The maximum output strain of an actuator could be 20%,¹³⁵ and an output force of 1.8 MPa¹³⁶ can be achieved with a work density of 460 kJ/m³. By utilisation of an adjustable electric stimulation source, HGAs can achieve a highly controllable actuation state and tuneable actuation degree. Benefitting from these merits, these materials have potential for application in artificial muscles.

However, most HGAs depend on an aqueous environment, which creates two main challenges. First, the challenge for an ionic hydrogel is the leakage of solvent, which greatly affects the durability and stability of the actuator. Second, due to the slow water diffusion-induced hydrogel volume transition, the actuation process of a large-scale actuator is too slow to gain a real-time response, which caused a low strain rate (2%/s), low output power (2×10^{-4} W) and low efficiency (0.164%).¹³⁷

HASEL. HASEL actuators have large output strains as fluidic actuators and can contract or elongate linearly without relying on aided structures. For a HASEL single-unit actuator, the maximum output strain is 170%, and a stress of approximately 0.3 MPa can be achieved when operating under a load of 1.5 kg.¹⁰⁰ Furthermore, the Maxwell pressure exerted in a HASEL actuator is independent of the electrode area, and the actuation strain and output force can be scaled by adjusting the ratio of the electrode area to the total area of an elastomeric shell or pouch. The output strain and force could be designed according to the requirement based on various HASEL configurations. In contrast to soft fluidic actuators, where inefficiencies and losses arise from fluid transport through systems of channels, and the additional weight of the mechanisms for producing pressurised fluids, the HASEL actuators generate hydraulic pressure locally via electrostatic forces and pump the liquid in reduced distances, which yields a fast actuation rate to 2176%/s and high conversion efficiency of 21% (similar to those achieved by DEA actuators).¹³⁸ Due to the great reduction in the design complexity, system weight and viscous loss, a single-unit HASEL actuator provides peak specific power of 586 W/kg and generates work of 64.4 kJ/m³ during contraction.¹³⁸

However, the employment of liquid dielectrics in HASEL actuators increases the response speed and achieves high positional control. The thick elastomer shells (>1 mm) require high voltages to reach electric fields large enough for actuation, which have

magnitudes in unit kV. In addition, the relatively large spaces for electrodes will be a drawback for certain applications.

Summary. The comprehensive comparison results are summarised as follows:

1. PAMs, such as the McKibben artificial muscle, are similar to biological muscle, and the actuation parameters are superior to those of biological muscle, except for a slightly smaller strain. However, PAMs are limited by the hysteresis and heavy gas tank in practice.
2. SMAs, such as the NiTi type, have large advantages in terms of the stress, work density and specific power, which originate from their high elastic moduli. For the same reason, SMAs exhibit low strain. The relatively low strain rate and low efficiency are caused by the thermal actuation method.
3. e-EAPs exhibit superiorities in strain rate and efficiency, high work density and specific power. The strain that is exerted depends on the elastic moduli of the materials. DEA materials with low elastic moduli have higher strain, while RFP materials with high elastic moduli have lower strain. However, the electric field required for actuation is high.
4. i-EAPs are actuated by a much lower voltage than e-EAPs and offer performances that are similar to those of biological muscle. However, the strain rate is low due to the slow transport of ions in electrolytes, and the efficiencies of i-EAPs are low due to the low electromechanical coupling.
5. Newly developed actuators display excellent biocompatibility, especially in the HGA, which could be applied to delivering medicine. Newly developed actuators also have excellent scalability, which could amplify their output strain and force in macro-scale actuators. However, the values of actuation parameters are relatively low compared with the other actuator technologies.

Artificial actuators have advantages over biological muscle in terms of the actuation parameters but challenges always exist when these artificial actuator technologies are applied in practice. Thus, artificial muscles cannot replace or perform as biological muscle. Therefore, further exploration of actuators with high performances is needed.

Future directions

The future trends of artificial actuators can be expected to fall into three different categories: (1) development

of new methods for improving existing technologies, (2) application of bio-inspired design to artificial actuators and (3) establishment of bio-hybrid systems.

New methods for improving existing technologies

In the design of actuators for robotics, some methods have been proposed to eliminate the negative impact of actuation challenges. For conventional PAM-based robots, a power source for actuation, typically a gas tank, is required; it is often tethered to the robot. For untethered actuation, combustion-powered gas sources, which can release high amounts of energy and can scale with the size of the robot, were proposed. For example, 'Octobot' has self-contained aqueous hydrogen peroxide (H_2O_2), which acts as a combustion source to excite the interior pneumatics (Figure 8(a)).¹⁹⁰ For e-EAPs, the main drawback is their use of high voltage (>1 kV typically) due to the high electric field that is needed. Using thin layers or creating materials with high dielectric constants, the required high voltage can be reduced. For i-EAPs, the strain rates are small due to the internal resistance of the polymers and electrodes and the slow ion diffusion rates inside the polymer. By increasing the applied potential, reducing the actuator thickness, or closely positioning the electrodes, the resulting actuation rates can be substantially improved.^{70,124,191}

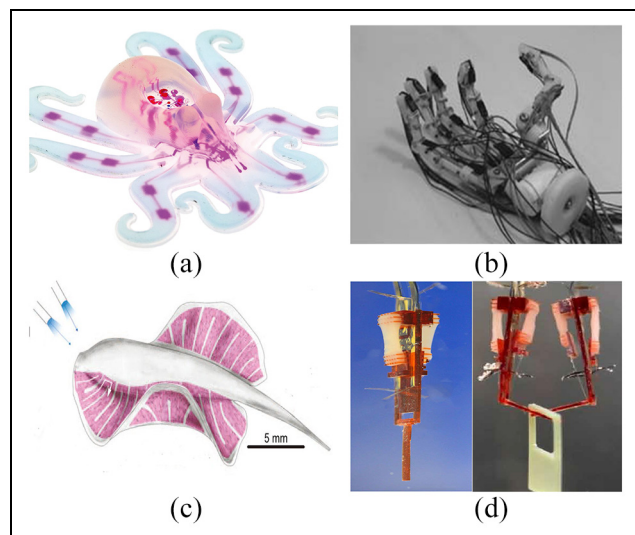


Figure 8. Future directions of robotic actuators: (a) combustion-powered robot—'Octobot', (b) self-adaption Yokoi hand, (c) cardiac muscle-based bio-hybrid robotic ray and (d) skeletal muscle-based antagonistic actuator. (a) reprinted with permission from Springer Nature, Nature, Copyright 2016;¹⁹⁰ (b) reprinted with permission from Springer Nature, Embodied artificial intelligence by F. Lida et al., Copyright 2004;¹⁹² (c) reprinted with permission from AAAS, Science, Copyright 2016;¹⁹³ and (d) reprinted with permission from AAAS, Science Robotics, Copyright 2018.¹⁹⁴

Bio-inspired design

Unlike conventional actuators, which are composed of separate modular systems for sensing, actuation and control, novel artificial actuators should perform as biological muscle, which is capable of synthesising these features into its material architecture. Another important property of biological muscle is its scalability, which allows it to actuate large- or small-scale biological mechanisms. Additional actuator specifications, such as dynamic responses and morphological compatibility, should be taken into account when designing a robot. Inspiration can be obtained from nature, and researchers can apply bio-inspired topology, geometry and material to artificial actuator design to achieve versatile functions and adaptive interactions.

Regarding natural mechanisms, in addition to the actuation function, the body also offers cognition and control functions to offload computation from the brain, which is also known as ‘morphological computation’. This process allows embodied agents, such as muscle, to not only function as actuators but also perform the task of sensing the environment and processing the information without participation of the brain.¹⁹⁵ For this reason, future artificial actuators could be combined with morphological computation, in which mechanical circuits are integrated such that the entire actuator can work as a computational resource for both perception and action. This actuation strategy would make the actuators work with rather than against their dynamics and reduce the complexity of the control architecture and the amount of computation, which enables more robust, faster and more efficient artificial actuator designs. In addition, based on the self-perception property, the morphological computation approach enables artificial actuators to switch their behaviours according to the environmental requirements. Artificial actuators can vary the stiffness distribution to satisfy the kinematic and dynamic requirements of the task. For example, the ‘Yokoi hand’, which is a 13 DOF robotic hand built from elastic and deformable materials for adjustment of its morphology to task requirements, can grasp different objects with the same simple control scheme (Figure 8(b)).¹⁹²

Bio-hybrid systems

Artificial actuators can also be formed by coupling bio-compatible synthetic materials with contractile muscle tissues to form a bio-hybrid system.¹⁹⁶ Bio-hybrid actuators feature the merits of biological muscle, which are capable of self-repair and self-assembly and can perform actuation the same as *in vivo*.^{197,198} However, we can control these bio-hybrid systems by external stimuli. For example, a jellyfish robot can be developed

by coupling a monolayer of anisotropic cardiomyocytes with a soft PDMS elastomer. When phototactically following a light cue, this robot exhibits natural kinematics and locomotion (Figure 8(c)).¹⁹³ Another bio-hybrid robot consists of an antagonistic pair of skeletal muscle tissue that is combined with a flexible hydrogel substrate, which enables large and long-term actuation of the muscle tissue, that is, $\sim 90^\circ$ rotation of a joint with almost 1-week lifetime (Figure 8(d)).¹⁹⁴ Thus, bio-hybrid actuators based on tissue engineering are promising candidates for enhancing robot performance.

Conclusion

This study has presented the main differences between biological muscle and conventional actuators in robots. These differences indicate that bio-inspired and biomimetic robots require more actuator options for reproducing natural movements. To identify actuators that can perform as biological muscle, this study has reviewed the artificial actuator technologies that are extensively employed in robotics. These actuators are also known as artificial muscles, whose actuation is based on pneumatic, thermal, photonic and electrical stimuli. No actuator can satisfy all the actuation requirements. The advantages and shortcomings of artificial actuators must be distinguished by comparing their actuation parameters, not only to provide guidelines for choosing appropriate actuator materials but also to provide targets that are aimed at improving these actuator technologies. According to the reviewed data, this study performed single parameter comparisons and comprehensive performance comparisons, which offer new insights into the way actuators were evaluated and selected in this study and indicate future possible directions for enhancing artificial actuator performance.

Author contributions

L.R. and Zh.Q. were involved in conceptualization; W.L. and Ky.W. were involved in methodology; W.L. and H.L. were involved in writing—original draft preparation; and Zh.Q., L.R. and Lq.R. were involved in funding acquisition.

Declaration of conflicting interests


The author(s) declared no potential conflicts of interest with respect to the research, authorship and/or publication of this article.

Funding

The author(s) disclosed receipt of the following financial support for the research, authorship and/or publication of this article: This research was funded by the project of National

Key R&D Programme of China (Nos. 2016YFE0103700 and 2018YFC2001300), National Natural Science Foundation of China (Nos. 91848204 and 51675222) and The Science and Technology Development Planning Project of Jilin Province (No. 20180101068JC).

ORCID iDs

Wei Liang  <https://orcid.org/0000-0002-5328-2545>

Hao Liu  <https://orcid.org/0000-0002-4816-7585>

References

1. Taylor AMKP. Science review of internal combustion engines. *Energ Pol* 2008; 36: 4657–4667.
2. Madden JDW. Mobile robots: motor challenges and materials solutions. *Science* 2007; 318: 1094–1097.
3. Ehsani M, Gao Y and Gay S. Characterization of electric motor drives for traction applications. In: *Proceedings of the IECON'03: 29th annual conference of the IEEE industrial electronics society (IEEE Cat. No. 03CH37468)*, Roanoke, VA, 2–6 November 2003, pp.891–896. New York: IEEE.
4. Amundson K, Raade J, Harding N, et al. Hybrid hydraulic-electric power unit for field and service robots. In: *Proceedings of the 2005 IEEE/RSJ international conference on intelligent robots and systems*, Edmonton, AB, Canada, 2–6 August 2005, pp.3453–3458. New York: IEEE.
5. Amundson K, Raade J, Harding N, et al. Development of hybrid hydraulic–electric power units for field and service robots. *Adv Robot* 2006; 20: 1015–1034.
6. Li Y, Li B, Ruan J, et al. Research of mammal bionic quadruped robots: a review. In: *Proceedings of the 2011 IEEE 5th international conference on robotics, automation and mechatronics (RAM)*, Qingdao, China, 17–19 September 2011, pp.166–171. New York: IEEE.
7. Atlas. The world's most dynamic humanoid robot, <https://www.bostondynamics.com/atlas> (2019, accessed 17 July 2019).
8. Trivedi D, Rahn CD, Kier WM, et al. Soft robotics: biological inspiration, state of the art, and future research. *Appl Bion Biomech* 2008; 5: 99–117.
9. Manti M, Cacucciolo V and Cianchetti M. Stiffening in soft robotics: a review of the state of the art. *IEEE Robot Autom Mag* 2016; 23: 93–106.
10. Coyle S, Majidi C, LeDuc P, et al. Bio-inspired soft robotics: material selection, actuation, and design. *Extrem Mech Lett* 2018; 22: 51–59.
11. Ewoldt RH. Extremely soft: design with rheologically complex fluids. *Soft Robot* 2014; 1: 12–20.
12. Majidi C. Soft robotics: a perspective – current trends and prospects for the future. *Soft Robot* 2014; 1: 5–11.
13. Nassar JM, Rojas JP, Hussain AM, et al. From stretchable to reconfigurable inorganic electronics. *Extrem Mech Lett* 2016; 9: 245–268.
14. Heping C, Fuhlbrigge T and Li XZ. Automated industrial robot path planning for spray painting process: a review. In: *Proceedings of the 2008 IEEE international conference on automation science and engineering*, Arlington, VA, 23–26 August 2008, pp.522–527. New York: IEEE.
15. Kalouche S. GOAT: a legged robot with 3D agility and virtual compliance. In: *Proceedings of the 2017 IEEE/RSJ international conference on intelligent robots and systems (IROS)*, Vancouver, BC, Canada, 24–28 September 2017, pp.4110–4117. New York: IEEE.
16. Dickinson MH. How animals move: an integrative view. *Science* 2000; 288: 100–106.
17. Pfeifer R and Gómez G. Morphological computation – connecting brain, body, and environment. In: Sendhoff B, Körner E and Sporns O (eds) *Creating brain-like intelligence*. Berlin: Springer, 2009, pp.66–83.
18. Hollerbach JM, Hunter IM and Ballentyne J. A comparative analysis of actuator technologies for robotics. *Robot Rev* 1991; 2: 299–342.
19. Mohd JJ, Leary M, Subic A, et al. A review of shape memory alloy research, applications and opportunities. *Mater Des* 2014; 56: 1078–1113.
20. Liu Z, Toh W and Ng TY. Advances in mechanics of soft materials: a review of large deformation behavior of hydrogels. *Int J Appl Mech* 2015; 7: 1530001.
21. Daerden F and Lefeber D. Pneumatic artificial muscles: actuators for robotics and automation. *Eur J Mech Eng* 2000; 47: 11–21.
22. Shin H, Ikemoto S and Hosoda K. Constructive understanding and reproduction of functions of gluteus medius by using a musculoskeletal walking robot. *Adv Robot* 2018; 32: 202–214.
23. Daerden F and Lefeber D. The concept and design of pleated pneumatic artificial muscles. *Int J Fluid Power* 2001; 2: 41–50.
24. Verrelst B, Ham RV, Vanderborgh B, et al. The pneumatic biped 'Lucy' actuated with pleated pneumatic artificial muscles. *Auton Robot* 2005; 18: 201–213.
25. Kukolj M. *Axially contractable actuator*. US4819547 Patent, 1989.
26. Krishnan G, Bishop-Moser J, Kim C, et al. Kinematics of a generalized class of pneumatic artificial muscles. *J Mech Robot* 2015; 7: 041014.
27. Sanan S, Lynn PS and Griffith ST. Pneumatic torsional actuators for inflatable robots. *J Mech Robot* 2014; 6: 031003.
28. Baldwin HA. Realizable models of muscle function. In: Baldwin HA (ed.) *Biomechanics*. New York: Springer, 1969, pp.139–147.
29. Winters JM. Braided artificial muscles: mechanical properties and future uses in prosthetics/orthotics. In: *Proceedings of the RESNA 13th annual conference*, Washington, DC, 15–20 June 1990, pp.173–174. Washington, DC: RESNA.
30. Wu M, Driver T, Wu SK, et al. Design and preliminary testing of a pneumatic muscle-actuated transfemoral prosthesis. *J Med Dev* 2014; 8: 044502.
31. Park YL, Chen B, Pérez-Arancibia NO, et al. Design and control of a bio-inspired soft wearable robotic device for ankle-foot rehabilitation. *Bioinspir Biomim* 2014; 9: 016007.
32. Daerden F. *Conception and realization of pleated pneumatic artificial muscles and their use as compliant actuation*

- elements. PhD Thesis, Vrije Universiteit Brussel, Brussels, 1999.
33. Yarlott JM. *Fluid actuator*. US3645173 Patent, 1972.
 34. Immea G. *Tentacle-like manipulators with adjustable tension lines*. US5317952 Patent, 1994.
 35. Henri MA. *Elastic diaphragm*. US2642091 Patent, 1953.
 36. Paynter HM. *High pressure fluid-driven tension actuators and method for constructing them*. US4751869 Patent, 1988.
 37. Kleinwächter H. *Device with a pressurizable variable capacity chamber for transforming a fluid pressure into a motion*. US3638536 Patent, 1972.
 38. Chou CP and Hannaford B. Measurement and modeling of McKibben pneumatic artificial muscles. *IEEE Trans Robot Autom* 1996; 12: 90–102.
 39. Sun L and Huang WM. Nature of the multistage transformation in shape memory alloys upon heating. *Met Sci Heat Treat* 2009; 51: 573–578.
 40. Mihálcz I. Fundamental characteristics and design method for nickel-titanium shape memory alloy. *Period Polytech Mech Eng* 2001; 45: 75–86.
 41. Lagoudas DC. *Shape memory alloys: modeling and engineering applications*. Berlin: Springer, 2008, pp.54–109.
 42. Perkins J. *Shape memory effects in alloys*. Berlin: Springer, 2012, pp.29–58.
 43. Villanueva A, Smith C and Priya S. A biomimetic robotic jellyfish (Robojelly) actuated by shape memory alloy composite actuators. *Bioinspir Biomim* 2011; 6: 036004.
 44. Kheirikhah MM, Rabiee S and Edalat ME. A review of shape memory alloy actuators in robotics. In: *Proceedings of the RoboCup 2010: robot soccer world cup XIV* (eds J Ruiz-del-Solar, E Chown and PG Plöger), Singapore, 19–25 June 2010, pp.206–217. Berlin: Springer.
 45. Festo. BionicOpter, https://www.festo.com/PDF_Flip/corp/Festo_BionicOpter/en/files/assets/basic-html/page-1.html (2019, accessed 17 July 2019).
 46. Price AD, Jnifene A and Naguib HE. Design and control of a shape memory alloy based dexterous robot hand. *Smart Mater Struct* 2007; 16: 1401.
 47. Enkovaara J, Ayuela A, Zayak AT, et al. Magnetically driven shape memory alloys. *Mater Sci Eng A* 2004; 378: 52–60.
 48. Tao T, Liang YC and Taya M. Bio-inspired actuating system for swimming using shape memory alloy composites. *Int J Autom Comput* 2006; 3: 366–373.
 49. Tickle R, James RD, Shield T, et al. Ferromagnetic shape memory in the NiMnGa system. *IEEE Trans Magn* 1999; 35: 4301–4310.
 50. Kanner OY, Shilo D, Sheng J, et al. Ferromagnetic shape memory flapper for remotely actuated propulsion systems. *Smart Mater Struct* 2013; 22: 085030.
 51. Carpi F, Kornbluh R, Sommer-Larsen P, et al. Electroactive polymer actuators as artificial muscles: are they ready for bioinspired applications? *Bioinspir Biomim* 2011; 6: 045006.
 52. Bar-Cohen Y. Electroactive polymers as artificial muscles: capabilities, potentials and challenges. In: *Proceedings of the Robotics 2000: fourth international conference and exposition/demonstration on robotics for challenging situations and environments* (ed. CS William), Albuquerque, NM, 27 February–2 March 2000, pp.188–196. Bellingham: SPIE.
 53. Kornbluh RD, Pelrine R, Pei Q, et al. Ultrahigh strain response of field-actuated elastomeric polymers. In: *Proceedings of the SPIE's 7th annual international symposium on smart structures and materials*, Newport Beach, CA, 7 June 2000, p.51. Bellingham: SPIE.
 54. Li T, Li G, Liang Y, et al. Fast-moving soft electronic fish. *Sci Adv* 2017; 3: e1602045.
 55. Zhao J, Niu J, McCoul D, et al. A rotary joint for a flapping wing actuated by dielectric elastomers: design and experiment. *Meccanica* 2015; 50: 2815–2824.
 56. Jung HS, Cho KH, Park JH, et al. Musclelike joint mechanism driven by dielectric elastomer actuator for robotic applications. *Smart Mater Struct* 2018; 27: 075011.
 57. Wang S, Huang B, McCoul D, et al. A soft breaststroke-inspired swimming robot actuated by dielectric elastomers. *Smart Mater Struct* 2019; 28: 045006.
 58. Nguyen CT, Phung H, Nguyen TD, et al. A small biomimetic quadruped robot driven by multistacked dielectric elastomer actuators. *Smart Mater Struct* 2014; 23: 065005.
 59. Gu G, Zou J, Zhao R, et al. Soft wall-climbing robots. *Sci Robot* 2018; 3: eaat2874.
 60. Nguyen CT, Phung H, Nguyen TD, et al. Multiple-degrees-of-freedom dielectric elastomer actuators for soft printable hexapod robot. *Sens Actuat A Phys* 2017; 267: 505–516.
 61. Mirfakhrai T, Madden JDW and Baughman RH. Polymer artificial muscles. *Mater Today* 2007; 10: 30–38.
 62. Breguet J, Johansson S, Driesen W, et al. A review on actuation principles for few cubic millimeter sized mobile micro-robots. In: *Proceedings of the 10th international conference on new actuators (Actuator 2006)*, Bremen, 14–16 June 2006, pp.374–381. Lausanne: INFO Science.
 63. Xiao P, Yi N, Zhang T, et al. Construction of a fish-like robot based on high performance graphene/PVDF bimorph actuation materials. *Adv Sci* 2016; 3: 1500438.
 64. Zhang Q. Electric EAP. In: Bar-Cohen Y (ed.) *Electroactive polymer (EAP) actuators as artificial muscle*. 2nd ed. Bellingham: SPIE, 2007, p.95.
 65. Madden JDW, Vandesteeg NA, Anquetil PA, et al. Artificial muscle technology: physical principles and naval prospects. *IEEE J Ocean Eng* 2004; 29: 706–728.
 66. Cheng ZY, Bharti V, Xu TB, et al. Electrostrictive poly(vinylidene fluoride-trifluoroethylene) copolymers. *Sens Actuat A Phys* 2001; 90: 138–147.
 67. Huang C, Klein R, Xia F, et al. Poly(vinylidene fluoride-trifluoroethylene) based high performance electroactive polymers. *IEEE Trans Dielectr Electr Insul* 2004; 11: 299–311.
 68. Andr JM and Delhalle J. *Quantum chemistry aided design of organic polymers: an introduction to the quantum chemistry of polymers and its applications*. Singapore: World Scientific, 1991.
 69. Pei Q and Inganaes O. Electrochemical applications of the bending beam method. 1. Mass transport and volume changes in polypyrrole during redox. *J Phys Chem* 1992; 96: 10507–10514.

70. Madden JD, Cush RA, Kanigan TS, et al. Fast contracting polypyrrole actuators. *Synth Met* 2000; 113: 185–192.
71. Okuzaki H and Kunugi T. Adsorption-induced chemomechanical behavior of polypyrrole films. *J Appl Polym Sci* 1997; 64: 383–388.
72. Moghadam AAA, Kouzani A, Torabi K, et al. Development of a novel soft parallel robot equipped with polymeric artificial muscles. *Smart Mater Struct* 2015; 24: 035017.
73. Chikhaoui MT, Cot A, Rabenorosoa K, et al. Design and closed-loop control of a tri-layer polypyrrole based telescopic soft robot. In: *Proceedings of the 2016 IEEE/RSJ international conference on intelligent robots and systems (IROS)*, Daejeon, Korea, 9–14 October 2016, pp.1145–1150. New York: IEEE.
74. McGovern S, Alici G, Truong VT, et al. Finding NEMO (novel electromaterial muscle oscillator): a polypyrrole powered robotic fish with real-time wireless speed and directional control. *Smart Mater Struct* 2009; 18: 095009.
75. McGovern ST, Abbot M, Emery R, et al. Evaluation of thrust force generated for a robotic fish propelled with polypyrrole actuators. *Polym Int* 2010; 59: 357–364.
76. Wang C, Nosaka T, Yost B, et al. Printed carbon nanotubes on polymer films for active origami. *Mater Res Lett* 2013; 1: 13–18.
77. Lima MD, Li N, Jung de Andrade M, et al. Electrically, chemically, and photonically powered torsional and tensile actuation of hybrid carbon nanotube yarn muscles. *Science* 2012; 338: 928–932.
78. Jung K, Nam J and Choi H. Investigations on actuation characteristics of IPMC artificial muscle actuator. *Sens Actuat A Phys* 2003; 107: 183–192.
79. Chen Z, Um TI and Bart-Smith H. Bio-inspired robotic manta ray powered by ionic polymer–metal composite artificial muscles. *Int J Smart Nano Mater* 2012; 3: 296–308.
80. Shen Q, Wang T, Liang J, et al. Hydrodynamic performance of a biomimetic robotic swimmer actuated by ionic polymer–metal composite. *Smart Mater Struct* 2013; 22: 075035.
81. Kim MH, Kim KY, Lee JH, et al. An experimental study of force control of an IPMC actuated two-link manipulator using time-delay control. *Smart Mater Struct* 2016; 25: 117001.
82. Billah MM, Khan R and Shafie AA. SMARS-I: smart material actuated robotic snake (ver-1). *Mater Today Proc* 2016; 3: 572–577.
83. Dresselhaus G and Iichiro S. *Physical properties of carbon nanotubes*. Singapore: World Scientific, 1998.
84. Baughman RH. Carbon nanotube actuators. *Science* 1999; 84: 1340–1344.
85. Chen L, Liu C, Liu K, et al. High-performance, low-voltage, and easy-operable bending actuator based on aligned carbon nanotube/polymer composites. *ACS Nano* 2011; 5: 1588–1593.
86. Foroughi J, Pinks GM, Wallace GG, et al. Torsional carbon nanotube artificial muscles. *Science* 2011; 334: 494–497.
87. Shahinpoor M and Kim KJ. Ionic polymer-metal composites: I. Fundamentals. *Smart Mater Struct* 2001; 10: 819–833.
88. Kim KJ and Shahinpoor M. Ionic polymer metal composites: II. Manufacturing techniques. *Smart Mater Struct* 2003; 12: 65–79.
89. Shahinpoor M. Mechano-electrical phenomena in ionic polymers. *Math Mech Solids* 2003; 8: 281–288.
90. Jain RK, Majumder S and Dutta A. SCARA based peg-in-hole assembly using compliant IPMC micro gripper. *Robot Auton Syst* 2013; 61: 297–311.
91. Jain RK, Patkar US and Majumdar S. Micro gripper for micromanipulation using IPMCs (ionic polymer metal composites). *J Sci Ind Res (India)* 2009; 68: 23–28.
92. Mirvakili SM and Hunter IW. Multidirectional artificial muscles from nylon. *Adv Mater* 2017; 29: 1604734.
93. Jia T, Wang Y, Dou Y, et al. Moisture sensitive smart yarns and textiles from self-balanced silk fiber muscles. *Adv Funct Mater* 2019; 29: 1808241.
94. Haines CS, Lima MD, Li N, et al. Artificial muscles from fishing line and sewing thread. *Science* 2014; 343: 868–872.
95. Wu L, Jung de Andrade M, Saharan LK, et al. Compact and low-cost humanoid hand powered by nylon artificial muscles. *Bioinspir Biomim* 2017; 12: 026004.
96. Almubarak Y and Tadesse Y. Twisted and coiled polymer (TCP) muscles embedded in silicone elastomer for use in soft robot. *Int J Intell Robot Appl* 2017; 1: 352–368.
97. Shi Q, Liu H, Tang D, et al. Bioactuators based on stimulus-responsive hydrogels and their emerging biomedical applications. *NPG Asia Mater* 2019; 11: 1–21.
98. Palteau E, Morales D, Dickey MD, et al. Reversible patterning and actuation of hydrogels by electrically assisted ionoprinting. *Nat Commun* 2013; 4: 1–7.
99. Sydney Gladman A, Matsumoto EA, Nuzzo RG, et al. Biomimetic 4D printing. *Nat Mater* 2016; 15: 413–418.
100. Acome E, Mitchell SK, Morrissey TG, et al. Hydraulically amplified self-healing electrostatic actuators with muscle-like performance. *Science* 2018; 359: 61–65.
101. Kellaris N, Venkata VG, Smith GM, et al. Peano-HASEL actuators: muscle-mimetic, electrohydraulic transducers that linearly contract on activation. *Sci Robot* 2018; 3: eaar3276.
102. Gupta P, Vermani K and Garg S. Hydrogels: from controlled release to pH-responsive drug delivery. *Drug Discov Today* 2002; 7: 569–579.
103. Koetting MC, Peters JT, Steichen SD, et al. Stimulus-responsive hydrogels: theory, modern advances, and applications. *Mater Sci Eng R Rep* 2015; 93: 1–49.
104. Stoychev G, Pureskiy N and Ionov L. Self-folding all-polymer thermoresponsive microcapsules. *Soft Matt* 2011; 7: 3277–3279.
105. Shiga T and Kurauchi T. Deformation of polyelectrolyte gels under the influence of electric field. *J Appl Polym Sci* 1990; 39: 2305–2320.
106. Gong JP, Nitta T and Osada Y. Electrokinetic modeling of the contractile phenomena of polyelectrolyte gels. One-dimensional capillary model. *J Phys Chem* 1994; 98: 9583–9587.
107. Hoare TR and Kohane DS. Hydrogels in drug delivery: progress and challenges. *Polymer (Guildf)* 2008; 49: 1993–2007.

108. Hunter IW and Lafontaine S. A comparison of muscle with artificial actuators. In: *Proceedings of the technical digest IEEE solid-state sensor and actuator workshop*, Hilton Head Island, SC, 22–25 June 1992, pp.178–185. New York: IEEE.
109. Bar-Cohen Y. Electroactive polymers as artificial muscles—reality and challenges. In: *Proceedings of the 19th AIAA applied aerodynamics conference*, Anaheim, CA, 11–14 June 2001, p.1492. Reston, VA: AIAA.
110. Caldwell DG, Tsagarakis N and Medrano-Cerda GA. Bio-mimetic actuators: polymeric pseudo muscular actuators and pneumatic muscle actuators for biological emulation. *Mechatronics* 2000; 10: 499–530.
111. Hannaford B and Winters J. Actuator properties and movement control: biological and technological models. In Winters JM and Woo SL (eds) *Multiple muscle systems*. New York: Springer, 1990, pp.101–120.
112. Lederlé S. *Issues in the design of shape memory alloy actuators*. PhD Thesis, Massachusetts Institute of Technology, Cambridge, MA, 2002.
113. Tadesse Y. Electroactive polymer and shape memory alloy actuators in biomimetics and humanoids. In: *Proceedings of the electroactive polymer actuators and devices (EAPAD) 2013* (ed. Y Bar-Cohen), San Diego, CA, 9 April 2013, vol. 8687, p.868709. Bellingham: SPIE.
114. Hunter IW, Lafontaine S, Hollerbach JM, et al. Fast reversible NiTi fibers for use in microrobotics. In: *Proceedings of the IEEE micro electro mechanical systems*, Nara, Japan, 30 January–2 February 1991, pp.166–170. New York: IEEE.
115. Jun HY, Rediniotis OK and Lagoudas DC. Development of a fuel-powered shape memory alloy actuator system: II. Fabrication and testing. *Smart Mater Struct* 2007; 16: S95–S107.
116. Kornbluh RD, Pelrine R, Pei Q, et al. Electroelastomers: applications of dielectric elastomer transducers for actuation, generation, and smart structures. In: *Proceedings of the smart structures and materials 2002: industrial and commercial applications of smart structures technologies* (ed. AY McGowan), San Diego, CA, 9 July 2002, vol. 4698, pp.254–270. Bellingham: SPIE.
117. Ha SM, Park IS, Wissler M, et al. High electromechanical performance of electroelastomers based on interpenetrating polymer networks. In: *Proceedings of the electroactive polymer actuators and devices (EAPAD) 2008* (ed. Y Bar-Cohen), San Diego, CA, 10 April 2008, vol. 6927, p.69272C. Bellingham: SPIE.
118. Pelrine R, Kornbluh RD, Pei Q, et al. Dielectric elastomer artificial muscle actuators: toward biomimetic motion. In: *Proceedings of the smart structures and materials 2002: electroactive polymer actuators and devices (EAPAD)* (ed. Y Bar-Cohen), San Diego, CA, 11 July 2002, vol. 4695, pp.126–137. Bellingham: SPIE.
119. Bharti V, Cheng ZY, Gross S, et al. High electrostrictive strain under high mechanical stress in electron-irradiated poly(vinylidene fluoride-trifluoroethylene) copolymer. *Appl Phys Lett* 1999; 75: 2653–2655.
120. Sencadas V, Lanceros-Méndez S and Mano J. Effect of the mechanical stretching on the ferroelectric properties of a (VDF/TrFE) (75/25) copolymer film. *Solid State Commun* 2004; 129: 5–8.
121. Nguyen H, Navid A and Pilon L. Pyroelectric energy converter using co-polymer P(VDF-TrFE) and Olsen cycle for waste heat energy harvesting. *Appl Therm Eng* 2010; 30: 2127–2137.
122. Bauer F. Review on the properties of the ferroelastomer polymers and some new recent developments. *Appl Phys A* 2012; 107: 567–573.
123. Pei Q, Pelrine R, Stanford S, et al. Electroelastomer rolls and their application for biomimetic walking robots. *Synth Met* 2003; 135: 129–131.
124. Zhang R, Lochmatter P, Kunz A, et al. Spring roll dielectric elastomer actuators for a portable force feedback glove. In: *Proceedings of the smart structures and materials 2006: electroactive polymer actuators and devices (EAPAD)* (ed. Y Bar-Cohen), San Diego, CA, 22 March 2006, vol. 6168, p.61681T. Bellingham: SPIE.
125. Baughman RH. Conducting polymer artificial muscles. *Synth Met* 1996; 78: 339–353.
126. Madden JDW, Schmid B, Hechinger M, et al. Application of polypyrrole actuators: feasibility of variable camber foils. *IEEE J Ocean Eng* 2004; 29: 738–749.
127. Madden JDW, Madden PG and Hunter IW. Conducting polymer actuators as engineering materials. In: *Proceedings of the smart structures and materials 2002: electroactive polymer actuators and devices (EAPAD)* (ed. Y Bar-Cohen), San Diego, CA, 11 July 2002, vol. 4695, pp.176–190. Bellingham: SPIE.
128. Baughman RH. Carbon nanotubes—the route toward applications. *Science* 2002; 297: 787–792.
129. Spinks GM, Wallace GG, Fifield LS, et al. Pneumatic carbon nanotube actuators. *Adv Mater* 2002; 14: 1728–1732.
130. Mirfakhrai T, Oh J, Kozlov M, et al. Electrochemical actuation of carbon nanotube yarns. *Smart Mater Struct* 2007; 16: S243–S249.
131. Madden JDW, Barisci JN, Anquetil PA, et al. Fast carbon nanotube charging and actuation. *Adv Mater* 2006; 18: 870–873.
132. Kamamichi N, Kaneda Y, Yamakita M, et al. Biped walking of passive dynamic walker with IPMC linear actuator. In: *Proceedings of the SICE 2003 annual conference*, Fukui, Japan, 4–6 August 2003, pp.166–170. Indiranagar, India: INFODOC.
133. Nemat-Nasser S. Micromechanics of actuation of ionic polymer-metal composites. *J Appl Phys* 2002; 92: 2899–2915.
134. Le X, Lu W, Zhang J, et al. Recent progress in biomimetic anisotropic hydrogel actuators. *Adv Sci* 2019; 6: 1801584.
135. Tang P, Yan H, Chen L, et al. Anisotropic nanocomposite hydrogels with enhanced actuating performance through aligned polymer networks. *Sci China Mater* 2020; 63: 832–841.
136. Bartholome C, Derré A, Roubeau O, et al. Electromechanical properties of nanotube-PVA composite actuator bimorphs. *Nanotechnology* 2008; 19: 325501.
137. Hwang T, Frank Z, Neubauer J, et al. High-performance polyvinyl chloride gel artificial muscle actuator

- with graphene oxide and plasticizer. *Sci Rep* 2019; 9: 1–9.
138. Wang X, Mitchell SK, Rumley EH, et al. High-strain Peano-HASEL actuators. *Adv Funct Mater* 2020; 30: 1908821.
 139. Ashley S. Artificial muscles. *Sci Am* 2003; 289: 52–59.
 140. Sangian D. *New types of McKibben artificial muscles*. PhD Thesis, University of Wollongong, Wollongong, NSW, Australia, 2016.
 141. Festo. BionicSoftHand, <https://www.festo.com/group/en/cms/13508.htm> (2019, accessed 17 July 2019).
 142. Shadow biomorphic arm, <https://robots.ieee.org/robots/shadow/?gallery=photo3> (2019, accessed 17 July 2019).
 143. Festo. Airic's arm, <https://www.festo.com/group/en/cms/10247.htm> (2019, accessed 17 July 2019).
 144. Tondu B, Ippolito S, Guiochet J, et al. A seven-degrees-of-freedom robot-arm driven by pneumatic artificial muscles for humanoid robots. *Int J Robot Res* 2005; 24: 257–274.
 145. Asano Y, Okada K and Inaba M. Design principles of a human mimetic humanoid: humanoid platform to study human intelligence and internal body system. *Sci Robot* 2017; 2: eaaq0899.
 146. Festo. BionicKangaroo, https://www.festo.com/net/SupportPortal/Files/334103/Festo_BionicKangaroo_en.pdf (2019, accessed 17 July 2019).
 147. Mamalis AG, Vogtlander LOG and Markopoulos A. Nanotechnology and nanostructured materials: trends in carbon nanotubes. *Precis Eng* 2004; 28: 16–30.
 148. Naresh C, Bose PSC and Rao CSP. Shape memory alloys: a state of art review. In: *Proceedings of the IOP conference series: materials science and engineering* (Paper No. 1), Bangalore, India, 14–16 July 2016, p.012054. Bangalore, India: IOP Publishing.
 149. Shiotsu A, Yamanaka M, Matsuyama Y, et al. Crawling and jumping soft robot KOHARO. In: *Proceedings of the 2005 international symposium on robotics*, Tokyo, Japan, 29 November–1 December 2005, p.134, Tokyo, Japan: Fraunhofer IPA.
 150. Andrianesis K and Tzes A. Design of an anthropomorphic prosthetic hand driven by shape memory alloy actuators. In: *Proceedings of the 2008 2nd IEEE RAS & EMBS international conference on biomedical robotics and biomechanics*, Scottsdale, AZ, 19–22 October 2008, pp.517–522. New York: IEEE.
 151. Sarban R, Jones RW, MacE BR, et al. A tubular dielectric elastomer actuator: fabrication, characterization and active vibration isolation. *Mech Syst Signal Pr* 2011; 25: 2879–2891.
 152. Sommer LP, Kofod G, Shridhar MH, et al. Performance of dielectric elastomer actuators and materials. In: *Proceedings of the smart structures and materials 2002: electroactive polymer actuators and devices (EAPAD)* (ed. Y Bar-Cohen), San Diego, CA, 9 July 2002, vol. 4695, pp.158–166. Bellingham: SPIE.
 153. Kovacs G, Lochmatter P and Wissler M. An arm wrestling robot driven by dielectric elastomer actuators. *Smart Mater Struct* 2007; 16: S306–S317.
 154. Cheng ZY, Xu H, Mai TX, et al. P(VDF-TrFE)-based electrostrictive co/ter-polymers and their device performance. In: *Proceedings of the smart structures and materials 2001: electroactive polymer actuators and devices* (ed. Y Bar-Cohen), San Diego, CA, 16 July 2001, vol. 4239, pp.106–116. Bellingham: SPIE.
 155. Xu H, Bai Y, Bharti V, et al. High dielectric constant composites based on metallophthalocyanine oligomer and poly(vinylidene fluoride-trifluoroethylene) copolymer. *J Appl Polym Sci* 2001; 82: 70–75.
 156. Carpi F and De Rossi D. Improvement of electromechanical actuating performances of a silicone dielectric elastomer by dispersion of titanium dioxide powder. *IEEE Trans Dielectr Electr Insul* 2005; 12: 835–843.
 157. Molberg M, Crespy D, Rupper P, et al. High breakdown field dielectric elastomer actuators using encapsulated polyaniline as high dielectric constant filler. *Adv Funct Mater* 2010; 20: 3280–3291.
 158. Zhang QM, Li H, Poh M, et al. An all-organic composite actuator material with a high dielectric constant. *Nature* 2002; 419: 284–287.
 159. Wiederkehr RS, Salvadori MC, Brugger J, et al. Fabrication and testing of a poly(vinylidene fluoride) (PVDF) microvalve for gas flow control. *Smart Mater Struct* 2007; 16: 2302.
 160. Lee CB and Tarbutton JA. Polyvinylidene fluoride (PVDF) direct printing for sensors and actuators. *Int J Adv Manuf Technol* 2019; 104: 3155–3162.
 161. Pelrine R, Kornbluh R, Joseph J, et al. High-field deformation of elastomeric dielectrics for actuators. *Mater Sci Eng C* 2000; 11: 89–100.
 162. Lee KKC, Munce NR, Shoa T, et al. Fabrication and characterization of laser-micromachined polypyrrole-based artificial muscle actuated catheters. *Sens Actuat A Phys* 2009; 153: 230–236.
 163. Mazzoldi A, Della SA and De-Rossi DE. Conducting polymer actuators: properties and modeling In: Osada Y and De Rossi DE (eds) *Polymer sensors and actuators*. Berlin: Springer, 2000, pp.207–244.
 164. Cole M and Madden JD. The effect of temperature exposure on polypyrrole actuation. *MRS Proc* 2005; 889: 0889-W04-04.
 165. Madden JD, Madden PG, Anquetil PA, et al. Load and time dependence of displacement in a conducting polymer actuator. In: *Proceedings of the materials research society symposium*, Warrendale, PA, 1–5 December 2002, pp.137–144. Boston, MA: Materials Research Society.
 166. Ikushima K, John S, Yokoyama K, et al. A practical multilayered conducting polymer actuator with scalable work output. *Smart Mater Struct* 2009; 18: 095022.
 167. Okuzaki H, Saido T, Suzuki H, et al. A biomorphic origami actuator fabricated by folding a conducting paper. *J Phys Conf Ser* 2008; 127: 012001.
 168. Lu W, Fadeev AG, Qi B, et al. Use of ionic liquids for π -conjugated polymer electrochemical devices. *Science* 2002; 297: 983–987.
 169. Ismail YA, Shin MK and Kim SJ. A nanofibrous hydrogel templated electrochemical actuator: from single mat to a rolled-up structure. *Sens Actuat B Chem* 2009; 136: 438–443.
 170. Ebbesen TW and Ajayan PM. Large-scale synthesis of carbon nanotubes. *Nature* 1992; 358: 220–222.

171. Thess A, Lee R, Nikolaev P, et al. Crystalline ropes of metallic carbon nanotubes. *Science* 1996; 273: 483–487.
172. Lee CJ, Lyu SC, Kim HW, et al. Large-scale production of aligned carbon nanotubes by the vapor phase growth method. *Chem Phys Lett* 2002; 359: 109–114.
173. Hahm G, Hashim DP, Vajtai R, et al. A review: controlled synthesis of vertically aligned carbon nanotubes. *Carbon Lett* 2011; 12: 185–193.
174. Gartstein YN, Zakhidov AA and Baughman RH. Mechanical and electromechanical coupling in carbon nanotube distortions. *Phys Rev B* 2003; 68: 115415.
175. Di J, Zhang X, Yong Z, et al. Carbon-nanotube fibers for wearable devices and smart textiles. *Adv Mater* 2016; 28: 10529–10538.
176. Cottinet PJ, Le MQ, Degraff J, et al. Strain phenomenon in carbon nanotube buckpaper actuator: experiments and modeling. *Sens Actuat A Phys* 2013; 194: 252–258.
177. Cottinet PJ, Souders C, Labrador D, et al. Nonlinear strain–electric field relationship of carbon nanotube buckypaper/Nafion actuators. *Sens Actuat A Phys* 2011; 170: 164–171.
178. Yang X, Wang W and Miao M. Moisture-responsive natural fiber coil-structured artificial muscles. *ACS Appl Mater Interf* 2018; 10: 32256–32264.
179. Yang X and Miao M. Carbon nanotube yarn-based actuators. In: Miao M (ed.) *Carbon nanotube fibers and yarns: production, properties and application in smart textiles*. Duxford: Woodhead Publishing, 2020, pp.271–291.
180. Hao M, Wang Y, Zhu Z, et al. A compact review of IPMC as soft actuator and sensor: current trends, challenges, and potential solutions from our recent work. *Front Robot AI* 2019; 6: 129.
181. Asaka K and Oguro K. Active microcatheter and biomedical soft devices based on IPMC actuators. In: Carpi F and Smela E (eds) *Biomedical applications of electroactive polymer actuators*. Chichester: John Wiley & Sons, 2009, pp.121–36.
182. Kim KJ and Shahinpoor M. A novel method of manufacturing three-dimensional ionic polymer-metal composites (IPMCs) biomimetic sensors, actuators and artificial muscles. *Polymer (Guildf)* 2002; 43: 797–802.
183. Palmre V, Hubbard JJ, Fleming M, et al. An IPMC-enabled bio-inspired bending/twisting fin for underwater applications. *Smart Mater Struct* 2012; 22: 014003.
184. Chen Z, Um TI and Bart-Smith H. Ionic polymer-metal composite enabled robotic manta ray. In: *Proceedings of the electroactive polymer actuators and devices (EAPAD)* (Paper No. 7976) (eds Y Bar-Cohen and F Carpi), San Diego, CA, 1 March 2011, p.797637. Bellingham: SPIE.
185. Yamakita M, Kamamichi N, Kaneda Y, et al. Development of an artificial muscle linear actuator using ionic polymer-metal composites. *Adv Robot* 2004; 18: 383–399.
186. Tomita N, Takagi K and Asaka K. Development of a quadruped soft robot with fully IPMC body. In: *Proceedings of the SICE annual conference 2011*, Tokyo, Japan, 13–18 September 2011, pp.1687–1690, Tokyo, Japan: INFODOC.
187. Nemat-Nasser S and Wu Y. Comparative experimental study of ionic polymer–metal composites with different backbone ionomers and in various cation forms. *J Appl Phys* 2003; 93: 5255–5267.
188. Maziz A, Concas A, Khaldi A, et al. Knitting and weaving artificial muscles. *Sci Adv* 2017; 3: e1600327.
189. Ozay O, Ekici S, Baran Y, et al. Removal of toxic metal ions with magnetic hydrogels. *Water Res* 2009; 43: 4403–4411.
190. Wehner M, Truby RL, Fitzgerald DJ, et al. An integrated design and fabrication strategy for entirely soft, autonomous robots. *Nature* 2016; 536: 451–455.
191. Ding J, Liu L, Spinks G, et al. High performance conducting polymer actuators utilising a tubular geometry and helical wire interconnects. *Synth Met* 2003; 138: 391–398.
192. Yokoi H, Arieta AH, Katoh R, et al. Mutual adaptation in a prosthetics application. In: Lida F, Pfeifer R, Steels L, et al. (eds) *Embodied artificial intelligence*. Berlin: Springer, 2004, pp.146–159.
193. Park SJ, Gazzola M, Park KS, et al. Phototactic guidance of a tissue-engineered soft-robotic ray. *Science* 2016; 353: 158–162.
194. Morimoto Y, Onoe H and Takeuchi S. Biohybrid robot powered by an antagonistic pair of skeletal muscle tissues. *Sci Robot* 2018; 3: eaat4440.
195. Pfeifer R, Lida F and Gómez G. Morphological computation for adaptive behavior and cognition. *Int Congr Ser* 2006; 1291: 22–29.
196. Anand SV and Saif TA. Emergent dynamics of cardiomyocyte clusters on deformable polymeric substrates. *Extrem Mech Lett* 2016; 8: 1–5.
197. Ricotti L and Menciassi A. Bio-hybrid muscle cell-based actuators. *Biomed Microdev* 2012; 14: 987–998.
198. Ricotti L, Trimmer B, Feinberg AW, et al. Biohybrid actuators for robotics: a review of devices actuated by living cells. *Sci Robot* 2017; 2: eaaq0495.